# A Computational Workbench Environment for Virtual Power Plant Simulation

**Quarterly Progress Report**

Reporting Period Start Date: April 1, 2002
Reporting Period End Date: June 30, 2002

Mike Bockelie, REI
Dave Swensen, REI
Martin Denison, REI
Connie Senior REI
Adel Sarofim REI
Bene Risio RECOM

July 28, 2002

DOE Cooperative Agreement No: DE-FC26-00NT41047

Reaction Engineering International
77 West 200 South, Suite 210
Salt Lake City, UT 84101

# Disclaimer

# Abstract

This is the seventh Quarterly Technical Report for DOE Cooperative Agreement No: DE-FC26-00NT41047. The goal of the project is to develop and demonstrate a computational workbench for simulating the performance of Vision 21 Power Plant Systems. Within the last quarter, good progress has been made on the development of our IGCC workbench. A series of parametric CFD simulations for single stage and two stage "generic" gasifier configurations have been performed. An advanced flowing slag model has been implemented into the CFD based gasifier model. A literature review has been performed on published gasification kinetics. Reactor models have been developed and implemented into the workbench for the majority of the heat exchangers, gas clean up system and power generation system for our Vision 21 reference configuration. Modifications to the software infrastructure of the workbench have been commenced to allow interfacing to the workbench reactor models that utilize the CAPE_Open software interface protocol.

# Table of Contents

# 1

# Executive Summary

The work to be conducted in this project received funding from the Department of Energy under Cooperative Agreement No: DE-FC26-00NT41047. This project has a period of performance that started on October 1, 2000 and continues through September 30, 2003.

The goal of the project is to develop and demonstrate a computational workbench for simulating the performance of Vision 21 Power Plant Systems. The Year One effort focused on developing a *prototype workbench* for the DOE Low-Emissions Boiler System (LEBS) Proof of Concept (POC) design. The Year Two effort is focused on developing a more advanced workbench environment for simulating a gasifier-based Vision 21 energyplex.

The main accomplishments during the last three months include:

- A series of parametric simulations for CFD models of a single stage (down fired) and a two stage (up fired) entrained flow gasifier have been performed. Variations in operating conditions included altering system pressure, fuel (coal) particle size and slurry/feed system properties. The conditions for our Vision 21 reference configuration were treated as the "baseline" operation.
- A flowing slag model has been implemented into the CFD based gasifier model. The model combines techniques originally developed under the US DOE HiPPS program and by the Collaborative Research Center for Coal and Sustainable Development (CCSD) in Australia. The slagging model is fully coupled to the CFD model and model verification is underway.
- A review of published gasification kinetics information has been performed.
- Reactor models have been developed and implemented into the workbench for most of the systems downstream of the gasifier for our Vision 21 reference configuration. The completed heat exchanger models include a gas recuperator, steam side cycle, and heat rescorvery steam generator (HRSG). The completed gas glean-up models include a cyclone (for particulate capture), syngas cooler, chlorine bed guard, bulk de-sulferizer and sulfur polisher. The completed power generation models include a steam generator and the expander and compressor portions of a gas turbine. Several of these reactor modules re-use software and sub-models from the prototype workbench developed during Year One of the program.
- Modifications to the software infrastructure of the IGCC workbench have been commenced to allow using reactor models that utilize the CAPE_Open software interface protocol.

Each of these topics is discussed in the following sections.

# 2

# Experimental Methods

Within this section we present brief discussions on the many sub-tasks that must be addressed in developing the workbench. For simplicity, the discussion items are presented in the order of the Tasks as outlined in our detailed Work Plan.

## Task 1 – Program Management

A presentation that highlighted material from this project was made at the ASME International Joint Power Generation Conference 2002 (IJPGC), held June 24-26, 2002 in Phoenix, Arizona.

- The paper, [Bockelie et al., 2002], was presented in a session dedicated to Advances in Fossil Fuel Plants. This paper provided an update on the development of our computational workbench including preliminary results for CFD models of downfired and upfired entrained flow gasifiers.

On May 6, 2002 project team members traveled to the DOE-NETL offices in Morgantown, WV to meet with our new DOE Project Officer in addition to other senior DOE personnel involved with the DOE Vision 21 program. The meeting provided us the opportunity to provide an overview of our project, current status of developing models and the workbench tool and to have initial discussions on models developed at DOE-NETL for Solid Oxide Fuel Cells and gas turbines.

On May 10, 2002 project team members met with Prof. John Stubington (University of New South Wales, Australia) from the Collaborative Research Center for Coal and Sustainable Development (CCSD) in Australia. Discussions focused on the status of our IGCC workbench tool and recent research and publications of the CCSD on coal gasification that will benefit this project.

# Task 2 – Virtual Plant Workbench II

The objective of this task is to further develop the capabilities of the computational workbench environment with the goal of providing the infrastructure needed to model a Vision 21 energyplex system. For the many sub-tasks contained under Task 2, the work effort is being performed by software engineers from Reaction Engineering International (REI) and Visual Influence (VI).

The main focus of this sub-task has been to continue to evolve a comprehensive software design, building on the ideas developed for Workbench I. As the complexity and capabilities of Workbench II continue to increase, the software design is evaluated and modified accordingly.

**Component Interfaces**

With the workbench capable of utilizing prototype CCA component-based models, we have now begun focusing on creating the infrastructure needed for using CAPE-OPEN compliant components. We view this as an important capability for the workbench as it will allow us access to a large number of process engineering models. As described below, we have made some initial progress toward making CAPE compliance a reality.

Recently, the official CAPE-OPEN website [http://www.colan.org] has finally made available two migration "wizards" to aide in the development of CAPE compliant package components. The first generates Visual Basic code for a CAPE unit operation while the second generates skeleton C++ code for CAPE properties. Utilizing these tools to provide component interface information, we were able to create a skeleton CAPE unit operation using a CORBA IDL. Note that CORBA has been used for this prototype implementation as a result of our workbench platform being Linux. Also note that although the Cape Open standard version 1.0 came out a couple of months ago, all the IDL specification and migration tools available are still for Version 0.93. Thus, all the work done is based on Version 0.93.

Now that we have implemented a skeleton CAPE unit operation, our plan is to create a CAPE version of the SCR model. Subsequent to this, we plan to move our thermodynamics database software into a CAPE thermo component. This modification will allow us to more closely follow the details of the CAPE specification during model development.

## Task 2.3 Module Implementation/Integration

The focus of this sub-task has been to continue the development of component wrappers needed for Workbench II computational components and to start integrating into the workbench component modules for equipment downstream.

**Thermodynamic Database:** With the large number of models being developed which rely on thermodynamic data, having each model provide its own properties database becomes impractical. To address this problem, we have developed an extensible thermodynamics abstract datatype component with methods and data targeted toward the calculations necessary for the workbench as a whole. This component is capable of providing extensive thermodynamic property information and also includes non-linear solvers for property calculations and a

chemical equilibrium solver. These capabilities will be continually enhanced to meet the needs of this project.

The thermodynamics component was designed to integrate with core SCIRun workbench functionality. As a result, all active modules can access a single component instance. Using this approach simplifies development of new models which need thermodynamic calculation capabilities, and makes much more efficient use of computer resources.

**Component Model Integration:** Component models for the chlorine guard bed, bulk desulfurizer, sulfur polisher, compressor/expander, cyclone and steam turbine have been integrated into the workbench. All are implemented directly with the use of C++ classes, and all but steam turbine utilize the functionality of the thermodynamic properties database.

**Gasifier Modification Tool:**

To provide the flexibility to investigate modified gasifier designs, a graphical tool has been implemented into the workbench that allows the user to easily rescale critical gasifier dimensions. In the last report we described our first version of the tool that was designed for use with a two-stage, upflow gasifier. During the last performance period we have extended the tool to also operate on a one stage, downflow gasifier. Starting with a computational mesh for the downflow gasifier, the user is able to choose key points on the gasifier profile and reposition (stretch) them. The repositioning can be performed by (1) selecting and dragging points/ranges with the mouse or (2) inputting exact measurements into data entry boxes. Complete testing of this feature is underway.

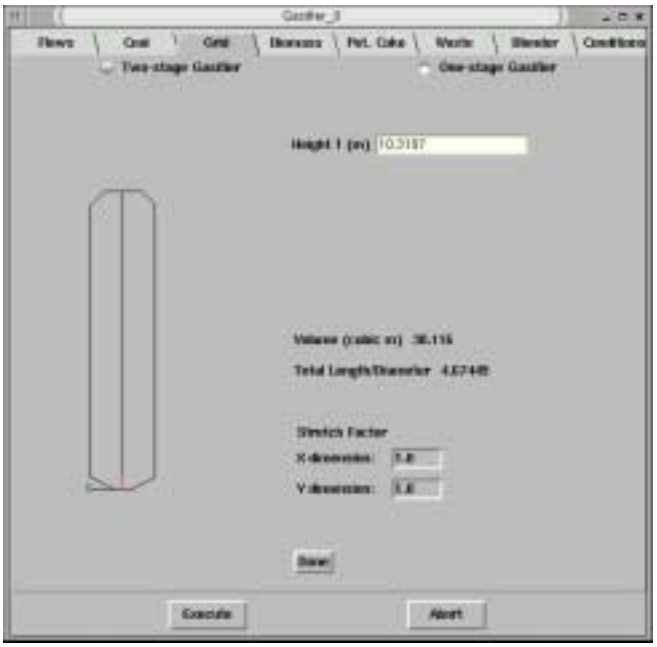


The gasifier modification tool is accessed through the User Interface (UI) button located on the gasifier module icon.

# Task 3 – Model Vision 21 Components

The purpose of this task is to develop the reactor and CFD models for the components that will be included in the workbench. In general, these models are first developed in a "stand-alone" form and then subsequently integrated into the workbench environment.

**Vision 21 Energy Plex Configuration**

Illustrated in Figure 1 is the Vision 21 energyplex configuration that the DOE Vision 21 Program Manager has suggested be used by this project to demonstrate the capabilities of our workbench environment. This configuration consists of an entrained flow gasifier, gas clean up system, gas turbines, heat recovery steam generator, steam turbine and SOFC fuel cells. As described below, a combination of CFD and reactor models will be used to simulate the performance of this configuration. A CFD model will be used for the entrained flow gasifier and simpler models will be used for the remainder of the equipment and processes.

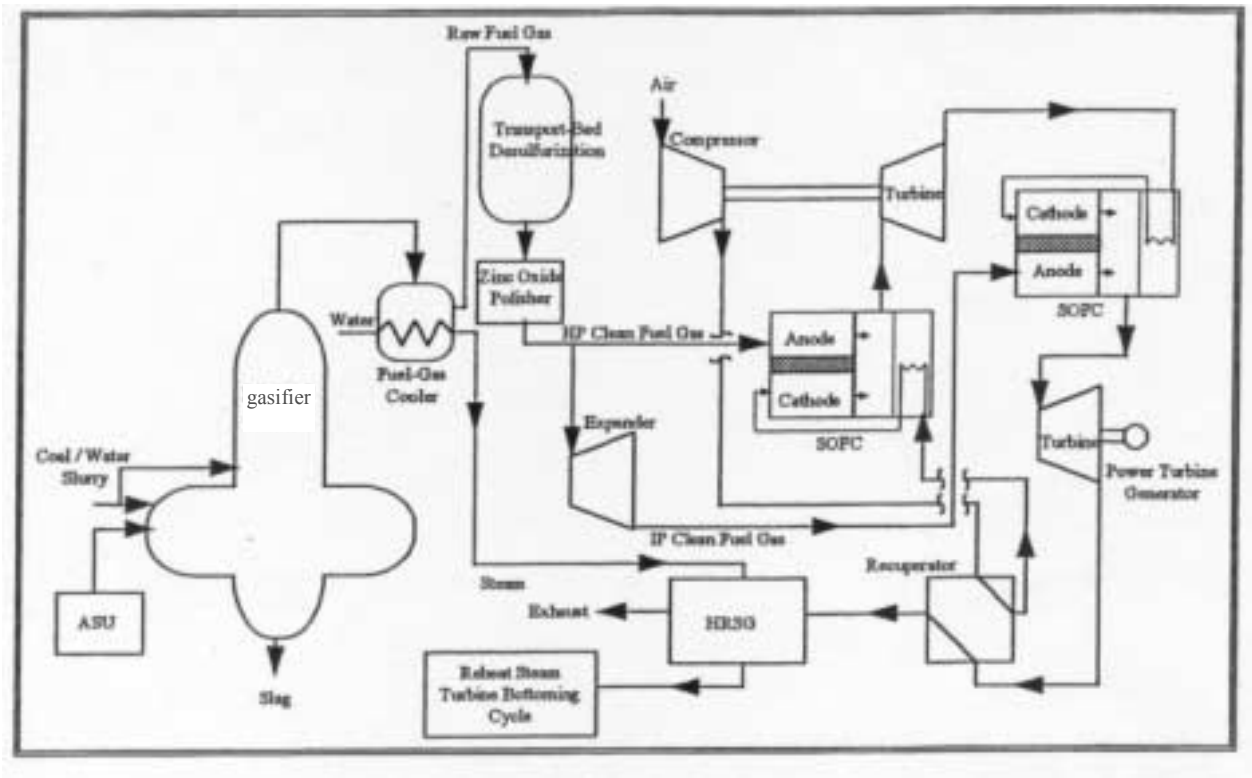


Figure 1. DOE selected Vision 21 test case configuration.

Listed in Tables 1 and 2 are the gross conditions for the configuration that were originally provided by DOE. Shown in Figure 2 is a mass and energy balance sheet obtained from DOE that provides more detailed information about the targeted Vision 21 configuration. A comparison of Figures 1 and 2 shows some discrepancies. As noted in previous progress reports, where information is missing we have used data available in the literature, combined with engineering judgment, to develop the required information to create the needed models.

**Table 1. Provided Operating Conditions for Vision 21 Energyplex**

| | |
|---|---|
| Gasifier (15 atm) | Two stage, up-fired |
| Coal Input to Gasifier (lb/hr) | 256,142 |
| Coal Type | Illinois #6 |
| Thermal Input (MW) | 875.8 |
| HP SOFC dc/ac | 189.4/182.8 |
| LP SOFC dc/ac | 121.4/117.2 |
| Gas Turbine, MW | 133.7 |
| Steam Turbine, MW | 118.0 |
| Fuel Expander, MW | 9.6 |
| Gross Power | 561.3 |
| Auxiliary Power, MW | 40.4 |
| Net Power, MW | 520.9 |
| Efficiency, % HHV | 59.5 |

**Table 2. Illinois Coal #6 Description**

| Proximate Analysis | As-Received (wt%) |
|---|---|
| Moisture | 11.12 |
| Ash | 9.70 |
| Volatile Matter | 34.99 |
| Fixed Carbon | 44.19 |
| TOTAL | 100.00 |
| HHV (Btu/lb) | 11666 |
| **Ultimate Analysis** | **As-Received (wt%)** |
| Moisture | 11.12 |
| Carbon | 63.75 |
| Hydrogen | 4.50 |
| Nitrogen | 1.25 |
| Sulfur | 0.29 |
| Ash | 9.70 |
| Oxygen (by difference) | 6.88 |
| TOTAL | 100.00 |

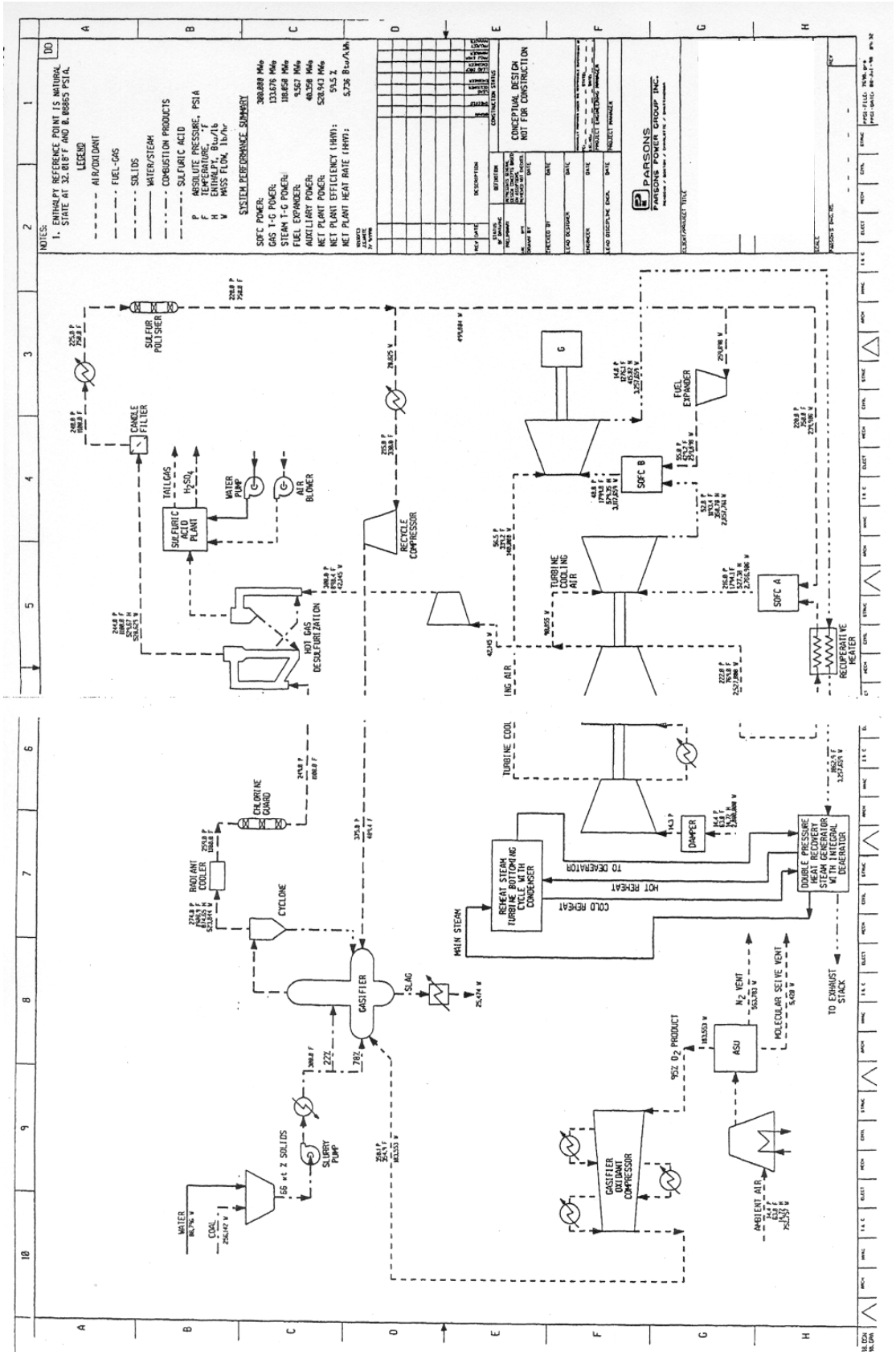


Figure 2. Mass and Energy Balance sheet provided by DOE for Vision 21 reference configuration.

## Task 3.3 Gasifier Models

Good progress has been made on developing CFD based models for entrained flow gasifiers. The models are being created using two different CFD codes. One gasifier model will be developed by REI personnel using *GLACIER*, a comprehensive two phase CFD based reacting CFD code. At present, *GLACIER* is limited to performing steady-state simulations and thus will be used to perform steady state CFD simulations of single and two stage gasifiers. The other gasifier model will be developed by RECOM using *AIOLOS*, a comprehensive reacting CFD code capable of performing transient boiler simulations and thus will be used to perform time dependent simulations for a single stage gasifier. Both CFD codes have been used to analyze numerous coal fired industrial combustion systems. The two codes employ different meshing technologies and different assumptions and sub-models for turbulence-chemistry interaction, simulating two-phase flow and reaction kinetics for combustion and gasification.

Below we highlight the progress within the last performance period in developing the CFD based gasifier models.

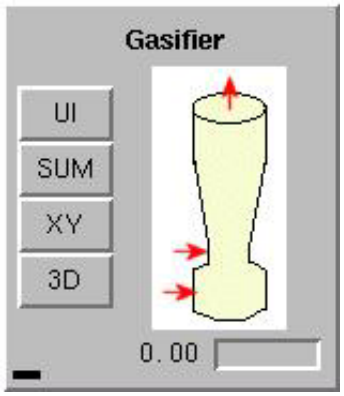


***GLACIER* Gasifier Module (Steady State):**. During the last performance period, the development efforts for this model have included completing incorporation of a CCA compliant *GLACIER* based gasifier module into the workbench, improvements to the User Interface for the *GLACIER* based gasifier module, continued investigations on published gasification reaction kinetics, incorporation of a slagging wall model into the gasifier model and commencing parametric simulations for a single and two stage gasifier. Details about the model development are described immediately below, whereas further details on the CFD model results are described in the Results and Discussion Section at the end of the report (see page **34**).

Slagging Wall Model

Slagging of hot mineral matter on the gasifier walls is important for good gasifier operation and thus is included within our comprehensive gasifier model. The slagging wall model we have implemented is an extension of work carried out by Physical Sciences Inc. and United Technologies Research Center under the US Department of Energy's Combustion 2000 program [Senior and Sangiovanni, 2001]; the Collaborative Research Center for Coal and Sustainable Development (CCSD) in Australia [CCSD], most notably Professor Terry Wall, Dr. David Harris and Mr. Peter Benyon; and researchers developing models for the Prenflo gasifier being used at the IGCC plant in Puertollano, Spain [Seggiani, 1998].

The model uses information from the gas flow field in the gasifier (e.g., gas composition, gas temperature, incident heat transfer, and particle deposition rate) to predict the slag properties (e.g., slag flow, slag thickness, frozen ash thickness) and heat transfer through the walls of the gasifier (for an assumed refractory resistance and external ambient temperature). The model is sufficiently general to include the effects of using a cooling jacket/system on the outside of the gasifier. The equations used to describe the ash layer are the conservation equations for momentum, energy, and mass. The model is two-dimensional. The slag thickness is calculated as a function of vertical distance down the walls. At each vertical location, the temperature profile is calculated through the layer thickness. The model is fully integrated into our CFD model of the gasifier. The slagging model can be applied to three-dimensional geometries by applying it for every vertical column of wall computational cells. A more detailed description of the model is provided below.

.

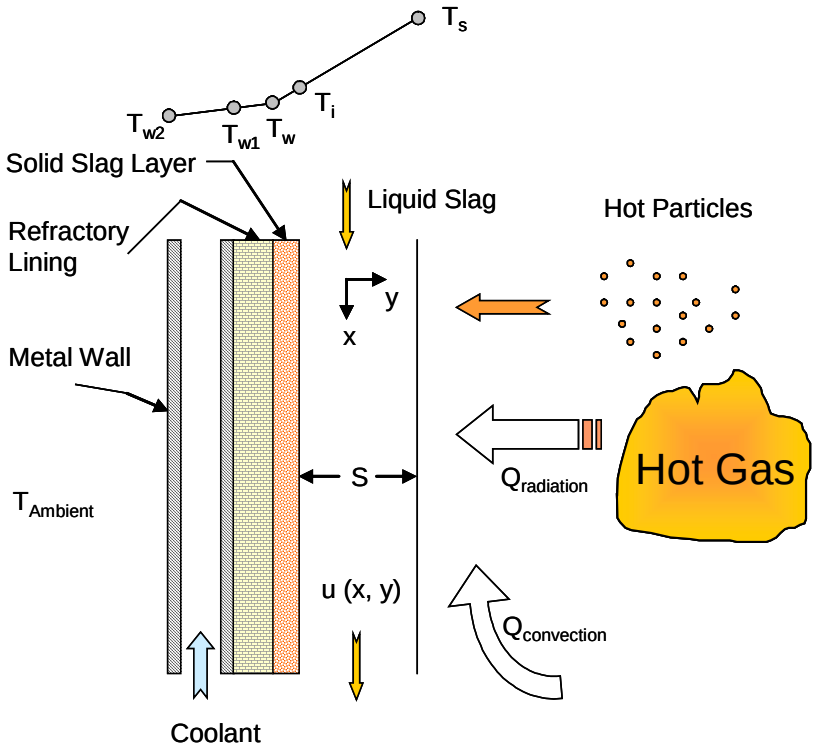


Figure 3. Gravity induced flow of a viscous slag layer down a solid surface.

Model Derivation

The flowing slag model treats the flow of slag on a vertical surface as shown in Figure 3. The equations used to describe the slag layer are the conservation equations for momentum, energy, and mass as first formulated by [Rogers, 1979]. Since inertial forces and the pressure gradient are negligible for a falling film at low Reynolds number with a free surface, the equation of motion (x-direction) for the slag layer is simply

$$\frac{\partial \tau}{\partial y} = \rho g \tag{1}$$

where $\tau$ and $\rho$ are the viscous shear stress and mass density of the slag layer, respectively, and g is the gravitational constant. By further assuming that the slag can be represented as a Newtonian fluid, the viscous shear stress for the slag is related to the viscosity, $\mu$, by the expression

$$\tau = \mu \frac{\partial u}{\partial y} \tag{2}$$

where u = u (x,y) is the velocity of the slag layer in the y-direction. The equation of motion can be rewritten as

$$\frac{\partial}{\partial y}\left( \mu \frac{\partial u}{\partial y} \right) = \rho g. \tag{3}$$

Since energy exchange due to convection and viscous dissipation is negligible for low Reynolds number flow and heat conduction across the slag layer is the dominant energy transport mechanism, the energy conservation equation for the slag layer is simply

$$q = k \frac{\partial T}{\partial y} \tag{4}$$

where q = q (x,y) is the heat flux normal to the slag layer, k is the thermal conductivity of the slag, and T = T (x,y) is the temperature of the slag.

The conservation of mass can be expressed as the integral of the velocity profile,

$$\dot{M}_S = \int_0^s \rho u(x,y) dy \tag{5}$$

where $\dot{M}_S$ is the mass flow per unit width of slag layer and the free surface of the slag layer is located at y = s. The mass flux is also equal to the integral of the ash deposition flux from the gas:

$$\dot{M}_S = \int_0^x \dot{m}_s(x) dx \tag{6}$$

where $\dot{m}_s(x)$ is the local ash deposition flux. If the viscosity of a portion of the slag layer is less than the critical viscosity, as indicated by the temperature of the layer, that portion of the layer is assumed to have frozen and the integral of equation (6) is only evaluated across the flowing portion of the slag. The boundary conditions can be stated as:

$$u(x,0) = 0 \tag{7}$$

$$T(x,0) = T_W(x) \tag{8}$$

$$\tau(x,s) = \tau_S(x, T_S) \tag{9}$$

$$q(x,s) = q_S(x, T_S) \tag{10}$$

where $T_s$ is the temperature at the slag surface. Equation (8) assumes that the wall temperature varies axially. Equations (9) and (10) require that we assume a surface shear force, $\tau_s$, and a surface heat flux, $q_s$, respectively.

A numerical solution was developed for the above set of equations which describe the development, flow, and heat transfer across a falling vertical slag layer. This numerical solution is based on transforming the governing equations with respect to the independent variables of the (x,y) coordinate system as follows:

$$\frac{\partial y}{\partial T} = \frac{k}{q(x,T)} \tag{11}$$

$$\frac{\partial u}{\partial T} = \frac{k\tau}{\mu\, q(x,T)} \tag{12}$$

$$\frac{\partial q}{\partial T} = 0 \tag{13}$$

Examination of equation (11) and the relevant boundary conditions leads to the following result

$$q(x,T) = q_S(x,T) \tag{14}$$

that is, the heat flux through the slag layer is equal to the heat flux at the surface of the layer. Integration of equation (11) gives the slag layer thickness, s, as

$$s(x) = \frac{k\,(T_s - T_w)}{q_s\,(x, T_s)} \tag{15}$$

To complete the slag layer model, the density, ρ, and thermal conductivity, k, of the slag are assumed to be constant and the free surface shear force is assumed to be zero, while the viscosity of the liquid slag is assumed to vary with temperature according to the Weymann relation which is expressed as:

$$\mu = A\,T\,e^{B/T} \qquad \text{for } T > T_{cv} \tag{16}$$

where A and B are coefficients for the particular ash. This approach was originally proposed by [Urbain et al.,1981] for the prediction of viscosities of ceramics, glasses and steel slags.

By transformation of the equation of motion, equation (3), using equation (11), and integrating with respect to temperature, one obtains the viscous shear stress in the slag layer given by

$$\tau(x, T) = \frac{\rho\, g\, k(T_S - T)}{q_S(x, T_S)} + \tau_S \qquad (17)$$

where $\tau_s = 0$.

Then by substituting equation (17) into equation (12) and integrating again with respect to temperature, the velocity profile for the liquid slag layer is given by

$$u(x, T) = \rho g \left[\frac{k}{q_S(x, T_S)}\right]^2 \int_{T_W}^{T} \frac{(T_S - \theta)}{A\, \theta^n\, e^{B/\theta}}\, d\theta \qquad (18)$$

Once the velocity is known, the mass flux can be calculated from equation (5) by the expression:

$$\dot{M}_s(x) = \frac{\rho k}{q_s(x, T_s)} \int_{T_i}^{T_s} u(x, \theta)\, d\theta \qquad (19)$$

where $T_i = T_w$ if there is no frozen slag layer. Otherwise $T_i$ is assumed to be equal to the temperature of critical viscosity.

In order to complete the description of slag flow behavior in a gasifier, a model describing the interactions between a gravity-induced flow of slag on a hot, vertical wall and heat transfer through the slag layer must take into consideration the viscous behavior of the slag.

Entrained-flow gasification units operate at high temperatures with the hot gases leaving the gasifier in the temperature range 1600 to 1800 K for a single stage gasifiers. Because of the high temperatures, mineral matter present in the coal forms slag. The ash slag flows down the refractory walls of the gasifier under the influence of gravity and is removed at the bottom of the gasifier after dropping into a water quench vessel. For these gasifiers to operate well, the slag must be removed continuously. The critical condition for continuous removal of the slag is the maintenance of the slag in a liquid phase so that it can flow unrestrictedly into the slag quench vessel. For this reason slag viscosity is an important property for determination of the performance of a given coal in a gasifier. As such, it is generally accepted that the optimum slag tapping viscosity is in the range 15 – 25 Pa·s at temperatures ranging from 1673 – 1773 K. It becomes apparent therefore, that the molten slag must have a low viscosity for good slag flow at the tapping temperature. The tapping temperature, however, must be high enough so as to avoid crystallization of the slag in the tapping hole but not high enough to have a negative impact on the cold gas efficiency of the gasifier. Therefore the removal of slag from a gasifier depends on the viscosity of the slag and the temperature at which the slag begins to crystallize.

A number of empirical correlations relating the viscosity of a slag to its composition and temperature have been reported in the literature. These include the correlations published by

[Reid and Cohen, 1944], [Hoy et al., 1965], [Watt, 1969], [Urbain et al., 1981] and [Schobert et al., 1985] for a variety of operating conditions.

Spurred by the need for prediction of viscosity of slags in entrained flow gasifiers, [Patterson et al., 2001] published an extensive report on the relationship between slag viscosity, ash composition and temperature for Australian coal ashes. The treatise is based on the modified Urbain model which yields viscosity-temperature relationships for gasifier slags with wt % FeO contents in the ranges 0-2.5, 2.5 – 5, 5 – 7.5, 7.5 – 10, 10 – 12.5, 12.5 – 15. In the present work these viscosity models have been incorporated in a CFD code for prediction of gasifier performance. Figures 4 and 5 show a comparison between predicted and experimental slag viscosities. The model considers the composition of the ash to be limited to the weight percent of the major species, namely, $SiO_2$, $Al_2O_3$, CaO and $F_2O_3$. In the model calculations, $Fe_2O_3$ is converted to FeO in order to account for the reducing environment in the gasifier.

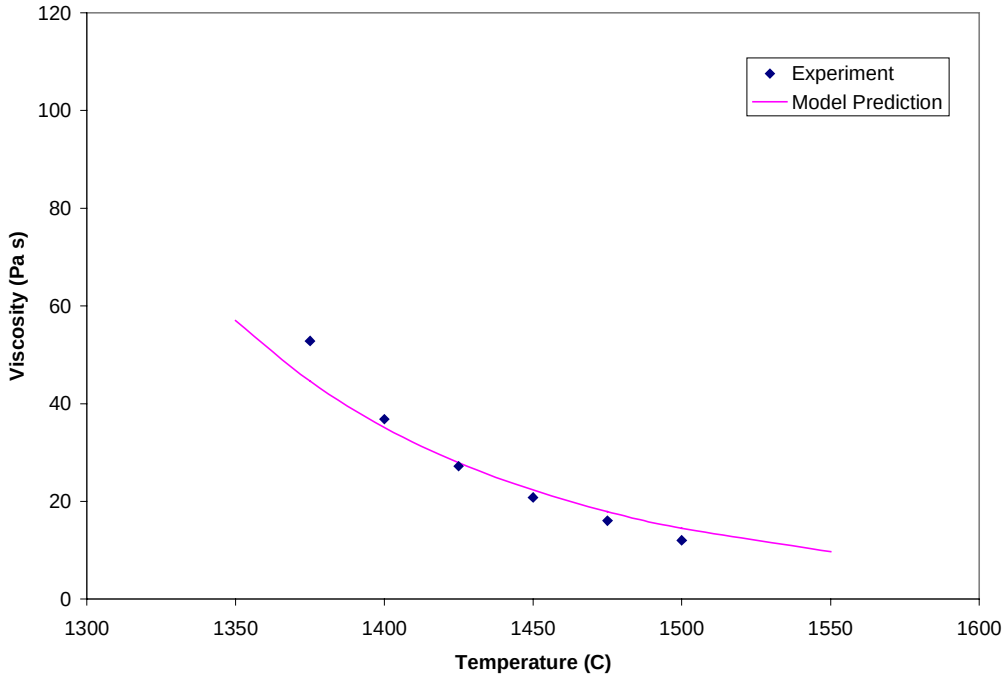


Figure 4. Predicted and experimental viscosities for a coal ash slag containing 52.2% $SiO_2$, 24.9% $Al_2O_3$, 4.83% CaO, 8.48% $Fe_2O_3$.

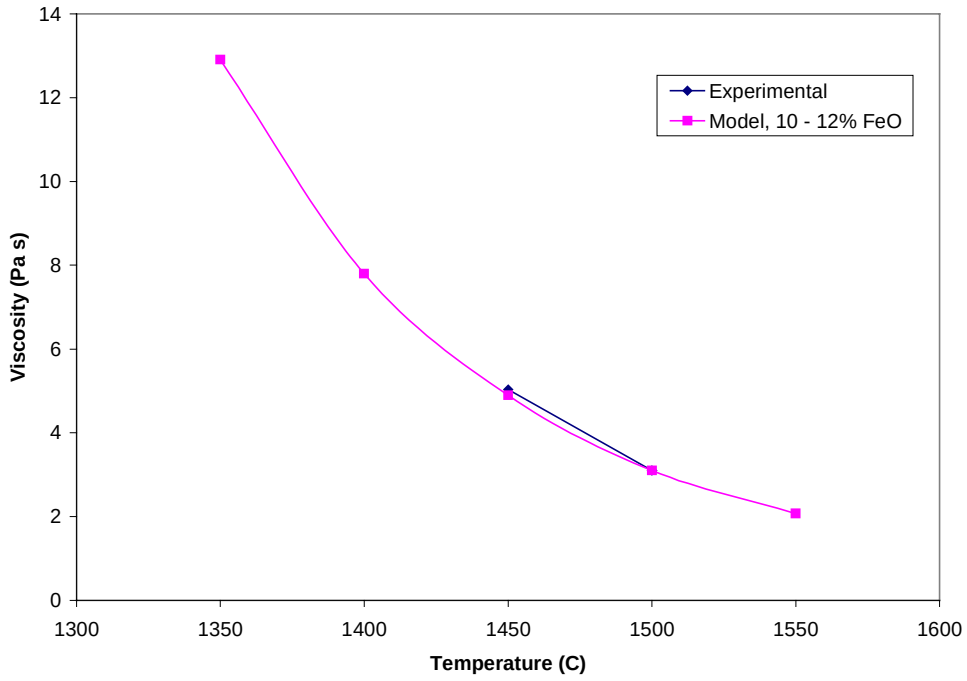


Figure 5. Predicted and experimental slag viscosities at 1723 and 1773 K. Coal ash contains 46.8% $SiO_2$, 23.16% $Al_2O_3$, 9.60% CaO and 11.56% $Fe_2O_3$.

The flow behavior of coal slags has been described in detail by [Watt, 1969]. Briefly, coal slags exhibit Newtonian flow at high temperatures where slag viscosity decreases with increase in temperature. However, if a Newtonian slag is cooled, its viscosity will increase until the fluid transforms to a Bingham plastic. Further slow cooling of the slag below a threshold temperature value will result in a sharp increase in viscosity, caused by the formation of crystals in the liquid. This viscosity is called the critical viscosity. The temperature at which this occurs is the highest temperature at which solid and liquid slag can co-exist in equilibrium and is called the temperature of critical viscosity, denoted by $T_{cv}$. If the slag is cooled even further beyond $T_{cv}$, more crystals will separate out and eventually the slag will become a solid.

The temperature of critical viscosity is a function of the ash composition. Estimation of the temperature of critical viscosity is a difficult proposition because a large number of data points covering a wide range of compositions is needed to provide a meaningful correlation. We have developed a correlation for $T_{cv}$ following the procedure laid out by [Hoy et al., 1965] and the slag data of [Patterson et al., 2001] given as

$$T_{cv}[K] = 3452 - 519.5\alpha + 74.5\alpha^2 - 67.8\beta + 0.86\beta^2 \qquad (20)$$

where $\alpha = SiO_2/Al_2O_3$ and $\beta = Fe_2O_3 + CaO + MgO$
$SiO_2 + Al_2O_3 + Fe_2O_3 + CaO + MgO = 100$ [weight%]

Figure 6 shows the relationship between the $T_{cv}$ correlation and the experimental data of [Patterson et al. , 2001].

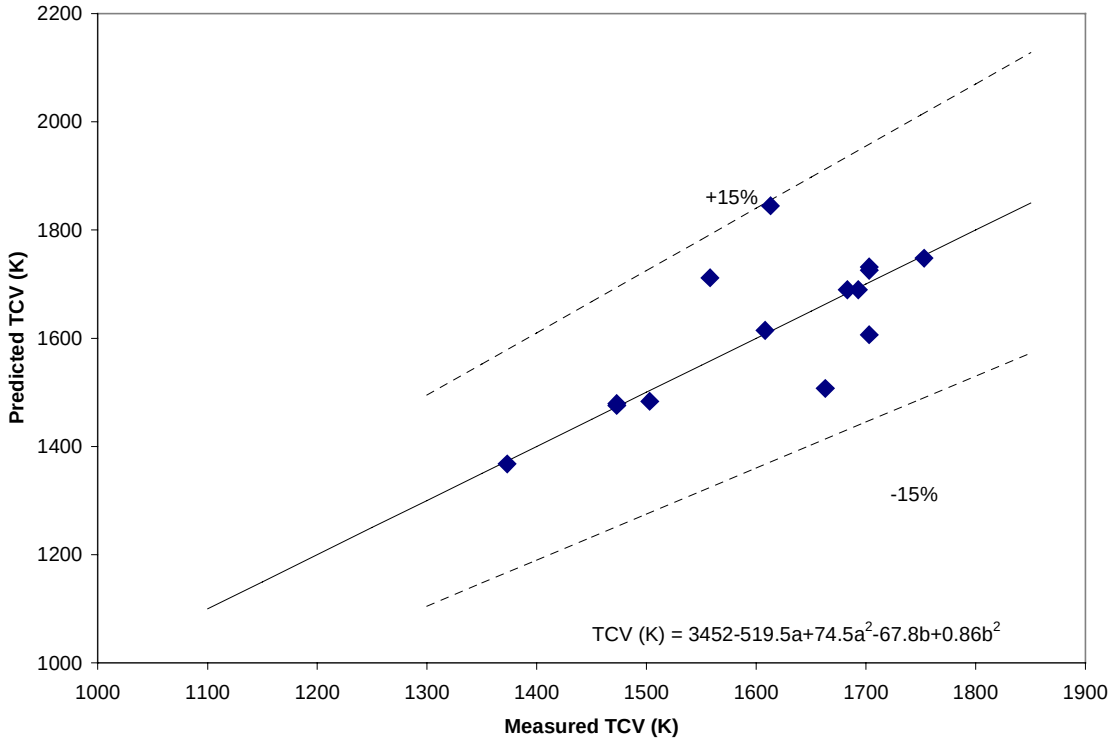


Figure 6. Correlation of predicted and measured temperature of critical viscosity for coal ash slags using experimental data of [Patterson et al, 2001].

Numerical Solution

The numerical procedure developed to simultaneously solve for the net radiant heat transfer to the wall, the liquid slag layer thickness and its related characteristics, at each axial position of the gasifier is as follows:

1. Assume the thickness of the liquid slag layer. At the top of the gasifier, at y = 0, the slag layer thickness is defined to be zero. For y>0, the slag layer thickness at the previous axial position is a good initial assumption for subsequent axial positions.

2. Using an iterative procedure based on the radiation and conduction equations, compute the surface temperature of the slag layer and the net heat flux to the wall slag surface.

3. Compute the velocity profile in the slag layer using equation (18).

4. Compute the mass flux of liquid slag using equation (19).

5. Compute the amount of slag which has frozen, as defined by the portion which is at a viscosity greater than the critical value. The temperature corresponding to the critical viscosity, $T_{cv}$, is used for this determination of the frozen slag fraction.

6. Compare the mass flux of liquid slag, computed in equation (3), with the sum of the deposition of ash from the gas phase which is in the slag layer, computed in equation (4). If these computed values for the slag mass flux agree within a reasonable tolerance (0.1% should be acceptable), the assumed slag layer thickness is correct.

7. Repeat the above procedure until accurate and consistent values have been found for the slag layer thickness and surface temperature.

CFD Implementation

The above flowing slag wall model has been integrated into the *GLACIER* gasifier model where the inputs (incident heat flux and particle deposition flux) needed for the slagging calculation are taken from the CFD heat transfer and particle calculations. The wall boundary of the gasifier model is divided into vertical strips, a slag calculation is performed as outlined above for each strip. The slag surface temperature solutions are then transferred back to the CFD heat transfer calculations as temperature boundary conditions. Iterations between the CFD and slagging model proceed until convergence.

Model Results

In this section, results for the 2-stage gasifier are presented. Figure 7 shows cross-sectional area averages of liquid and solid slag thickness as functions of the gasifier height. Slag formed only in the combustor section. Liquid slag thickness is in an order of a few millimeters, which is similar to that reported in Benyon et al. (2000), who simulated slag behavior in an air-blown gasifier with a similar geometry as used in this work. Solid slag also formed in the lower section of the gasifier, where the wall temperature changed dramatically, as shown in Figure 8. $T_s$ and $T_i$ in the figure denote liquid slag surface temperature and liquid-solid slag interface temperature, respectively. Figure 9 shows local slag thickness; the horizontal axis represents radial location of the gasifier, starting from the center of one of the injectors in the combustor section and moving counterclockwise. A few vertical strips of liquid slag can be observed; these strips locate above the middle-level injectors. Solid slag mainly formed in the section between the lowest-level injectors and the middle-level injectors, and in a region above the highest-level injectors.

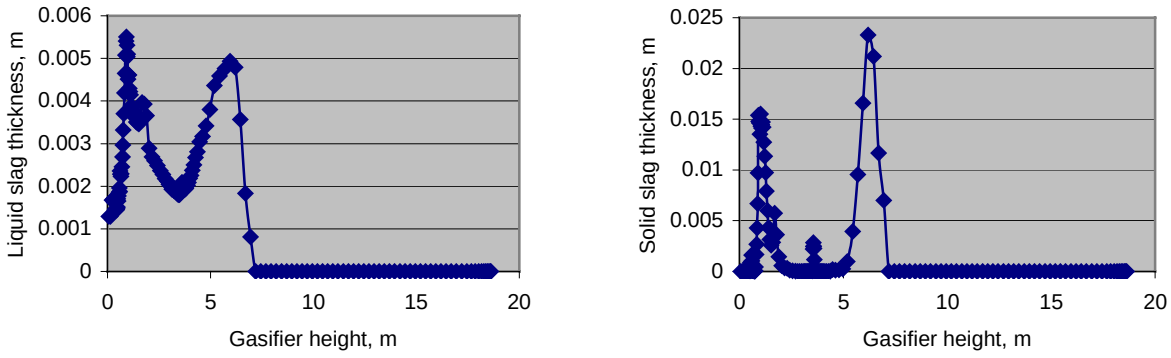


Figure 7. Average slag thickness as a function of gasifier height.

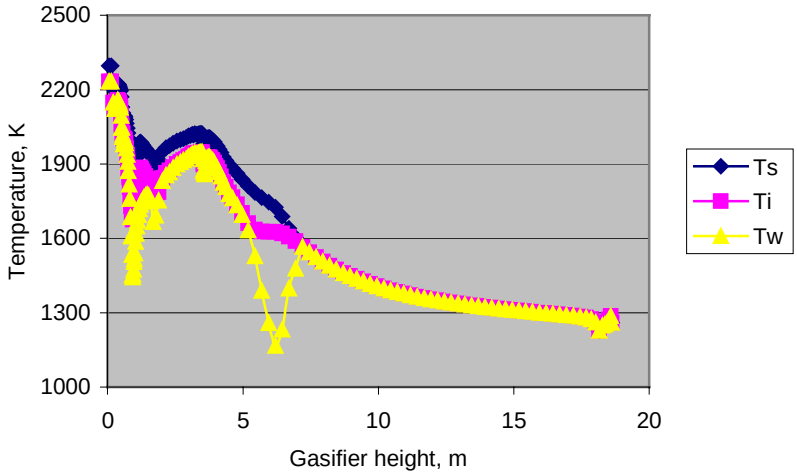


Figure 8. Average liquid slag surface temperature, liquid-solid slag interface temperature and wall temperature as functions of gasifier height.

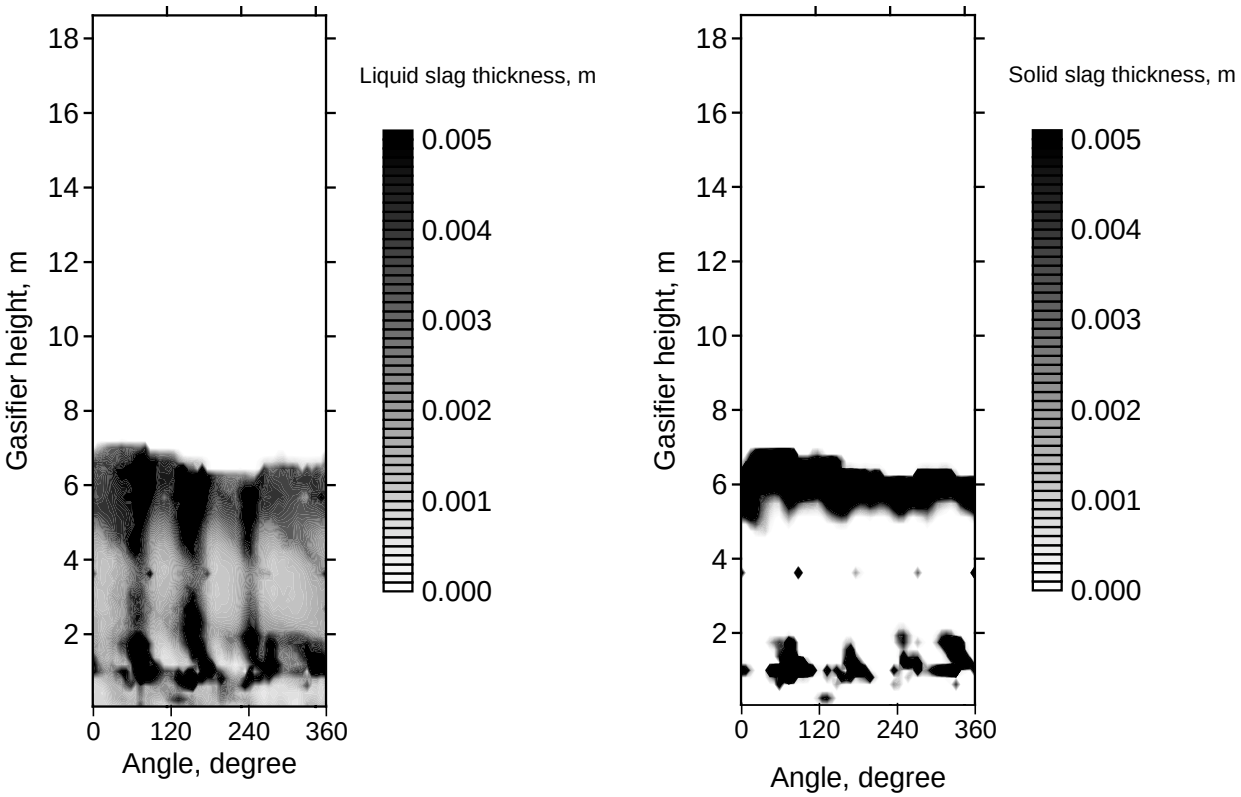


Figure 9. Local liquid and solid slag thickness.

High Pressure Gasification Kinetics

There is an extensive literature on the kinetics of devolatilization and gasification. Much of it is directed at the early moving bed and fluidized bed gasifiers and therefore is not directly relevant to entrained flow gasifiers, that involve higher temperatures and shorter residence times than packed and fluidized bed gasifiers. The literature on entrained flow gasification is limited; furthermore, some of the gasification kinetics at high pressures have been carried out on char samples generated at atmospheric pressure or slow heating conditions and that are therefore not representative of chars present in entrained flow gasifiers. In the current work, we draw extensively on an ongoing effort on gasification kinetics being carried out in Australia under the directions of Dr. David Harris at the CSIRO and Prof. Terry Wall at the University of Newcastle. The Australian data constitute one of the best sources of information and we have ready access to the information through a Memorandum of understanding between REI and the Collaborative Research Center for Sustainable Development (CCSD).

Devolatilization

Thermal decomposition kinetics is fast at entrained gasification temperatures and is not a strong function of pressure. Volatile yields are suppressed because volatile transport out of coal particles is inhibited as the pressure is increased. Many models have been developed for devolatilization, which give the rate, volatile yield and composition of the products. The three most widely used are these developed by Solomon and co-workers (1988, 1992), Niksa and Kerstein (1991), and Fletcher and Pugmire (1990). The models yield relatively comparable results. We have chosen the Chemical Percolation Devolatilization (CPD) model of Fletcher and Pugmire to provide information of importance to gasification such as tar yields, since it is in the public domain. The model also provides the effect of pressure on volatile yields. The results from the Fletcher and Pugmire model on the effect of pressure on volatile yields is compared in Figure 10 with data and correlations from a number of different investigations.

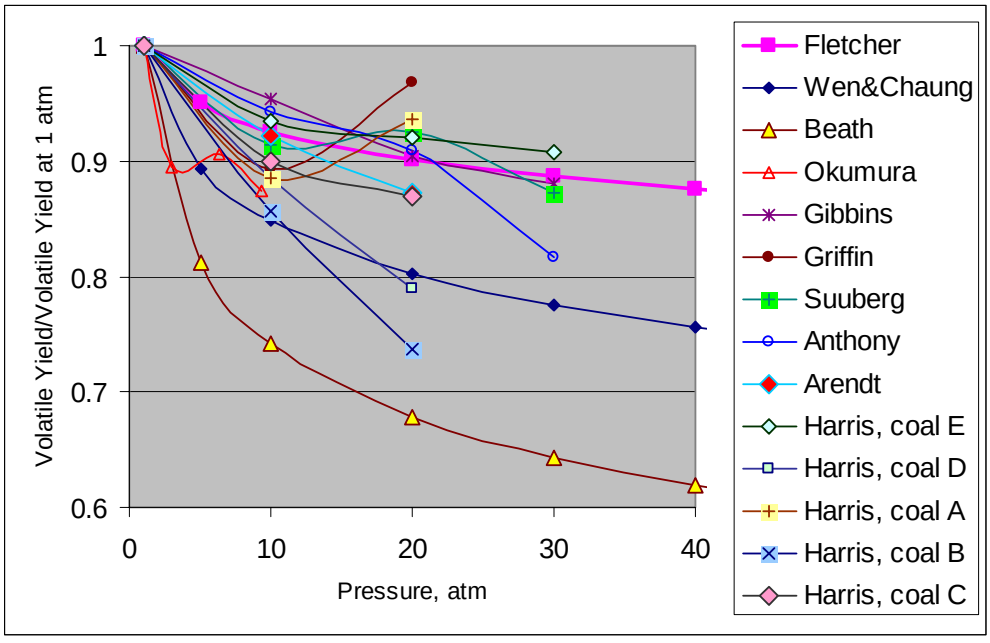


Figure 10. Comparison of model prediction of volatile yields with experimental data.

The CPD model tends to under-predict the decrease in volatile yields with increasing pressure, over a range of pressure from 1 to 30 atm, using a variety of coals. Included in the figure is the correlation by Wen and Chaung (1979), based on the data of Anthony et al. (1976) over the range of 0.1 to 50 atm:

$$\frac{V_p}{V_{p=1}} = 1 - 0.066 \ln P_t \qquad (21)$$

where $P_t$ is the total pressure in atmospheres.Wen and Chaung's model slightly over-predicts volatile yields at high pressures. Another correlation, by Beath, significantly over-predicts the effect of pressure on volatile yields. The future studies at the CCSD, involving entrained flow gasification, will help resolve the discrepancies between different correlations.

The two competing reaction pathway developed by Kobayashi et al. (1976) was used to model the gasification kinetics in the CFD code. The input parameters to the code are, however, modified to allow for the above dependence on pressure of volatile yields.

Char Morphology

The more important effect of total pressure on devolatilization is that on the morphology and reactivity of the product char. Because of the inhibition of volatile transport out of particles during devolatilization, the particles produced at high pressures have a higher percentage of particles with large macropores but with less micropores. The chars produced at high pressures contain a high percentage of cenospheric particles, classified as Group I by Wall et al. (2002). They developed a correlation for the effect of pressure on the fraction of particles forming cenosphere, $f_{ce}$. It is

$$f_{ce} = 0.006 P_t + 0.0053 vitr + 0.37 \qquad (22)$$

where $P_t$ is the total pressure in atmospheres and *vitr* is the volume percentage of vitrinite content of coal. For a gasifier operated at 25 atmospheres with a bituminous coal having 80 percent vitrinite, all of the particles are predicted to be present as cenospheres. For a lower vitrinite content of 50 percent, again at 25 atmospheres, 75 percent of the particles are predicted to be present as cenospheres. The increase in cenosphere content with increasing pressure increases the char fragmentation during gasification with an attendant increase on char reaction rates (Benfell et al., 2000) and a decrease in the particle size of ash produced (Wu et al., 2000).

The microporosity and therefore total surface area of the char are also impacted by the increase in total pressure. These changes in surface area and porosity will also influence the high pressure reactivity of the chars (Benfell et al., 2000). A further complication on structure is provided by the annealing and deactivation of the carbon structure with increasing exposure to high temperatures (Hurt et al., 1998; Seneca et al., 1998). Such deactivation needs to be considered at the longer residence times in the two-stage gasifier and potentially for char that is recycled.

Kinetics of Char Gasification

Having the correct gasification kinetics is critical for any gasifier model. Kinetics are needed to size the gasifier/combustor and determine the char combustion efficiency and possible char recycle requirements. The three reactants of importance are $O_2$, $H_2O$, and $CO_2$, with the possible addition of $H_2$ that can contribute to the formation of $CH_4$ at high pressures. The kinetics are determined by three resistances, that of external diffusion of the gas phase reactants to the particle surface and diffusion of the reactants from the surface, diffusion through the porous structure of the char, and reaction at the internal (mostly) and external char surface.

The external rate of diffusion is given by (Smith, 1982),

$$R_D = 0.75 D_i \left(\frac{P_0}{P_t}\right)\left(\frac{T_m}{T_0}\right)^{1.75} \frac{(C_i - C_s)}{d_p} \tag{23}$$

where the diffusion rate is in kg/m$^2$.s, $T_m$ is the average temperature of the boundary layer around the particle, and the subscript 0 denotes the reference conditions. For $P_0$ = 1 bar and $T_0$ = 1500 K, $D_i = 3.1\times10^{-4}$ m$^2$/s for $O_2$. $C_i$, $C_s$, and $d_p$ in the above equation are the reactant concentrations in the gas phase and particle surface and the particle diameter, respectively.

The reaction at the internal char surface, called the intrinsic kinetics, is a more fundamental property of the char as it permits the calculation of the effects on total reaction of changing char structure and surface area. Values for the intrinsic rate for a range of pressures are given by the Australian researchers (Benfell et al., 2000; Roberts and Harris, 2000), together with models on how the rates can be converted to the effective surface rate (Liu et al., 2000). One of the advantages of the more fundamental rate expression is that it can permit the determination of the effect of the change in internal pore structure with conversion. Such models have been used to determine the change of reactivity with changing conversion, where there is an initial increase in rate with conversion as the result of the increase in surface area as pores enlarge, followed by a decrease as pores overlap [Liu, et al., 2000].

The intrinsic kinetics that need to be used in such models are complicated by the adsorption/desorption kinetics at sites with a range of activities. The Langmuir-Hinshelwood model is found to still provide a simple representation of the competition of different reactants with the surface. For the $CO_2$-char reaction, for example, it provides the following relationship for the reaction rate

$$R_c = \frac{k_a p_{CO_2}}{1 + k_b p_{CO_2} + k_c p_{CO}} \tag{24}$$

The denominator represents the inhibition of the reaction as a result of adsorption on reactive surface sites by reactants and products. The number of terms in the denominator will increase in a product mixture containing other species that can be adsorbed on surface sites, such as $H_2O$. As a consequence of the inhibiting factor of adsorbed species, the order of the reaction between $CO_2$ and carbon decreases with increasing pressure (Roberts et al, 2001). This is a reason,

additional to the changes in char morphology with pressure, that it is difficult to extrapolate kinetics from atmospheric to higher pressures.

The intrinsic reaction rates of oxygen with carbon can be factors $10^3$ to $10^5$ higher than those of $H_2O$ and $CO_2$ [Harris and Smith, 1990; Roberts and Harris, 2000], but these differences decrease to factors less than ten at the higher temperatures in oxygen-blown gasifiers since the activation energies for $CO_2$ and $H_2O$ are higher than those of $O_2$ (see Figures 11 and 12). When allowance is made for diffusion within pores and in the particle boundary layer, the differences between the rates of the exothermic $O_2$/C reaction and the endothermic $CO_2$/C and $H_2O$/C become much smaller. But it is usually the case that the reaction of oxygen with carbon precedes those of $CO_2$ and $H_2O$.

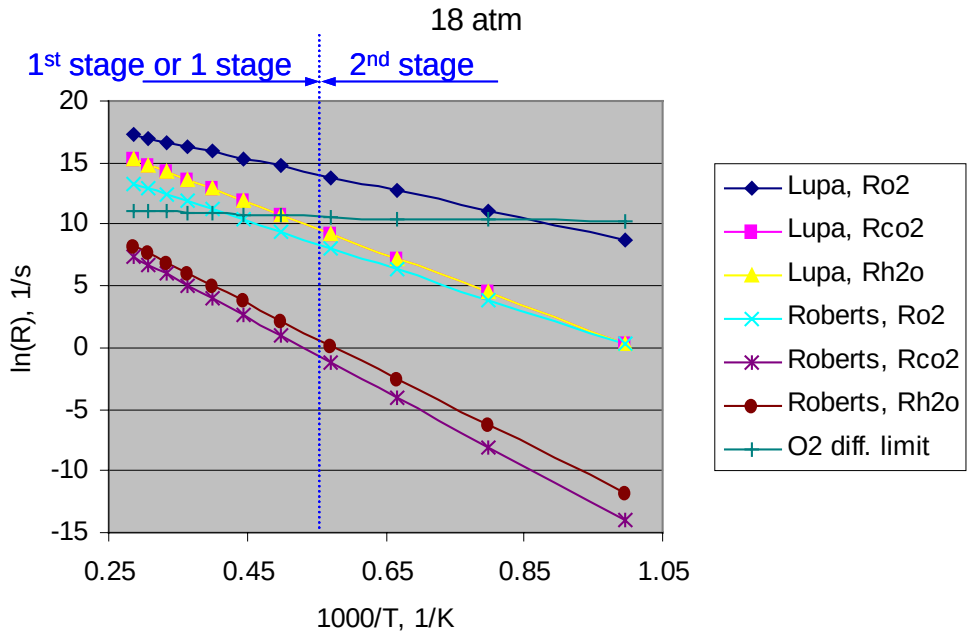


Figure 11. Comparison of the rates at 18 atmospheres from Lupa et al. (1979) and Roberts and Harris (2000) for the apparent reaction rates of $O_2$, $CO_2$, and $H_2O$ (each with a mole fraction of 0.2) with the mass transfer controlled rate for oxygen (also with a mole fraction of 0.2).

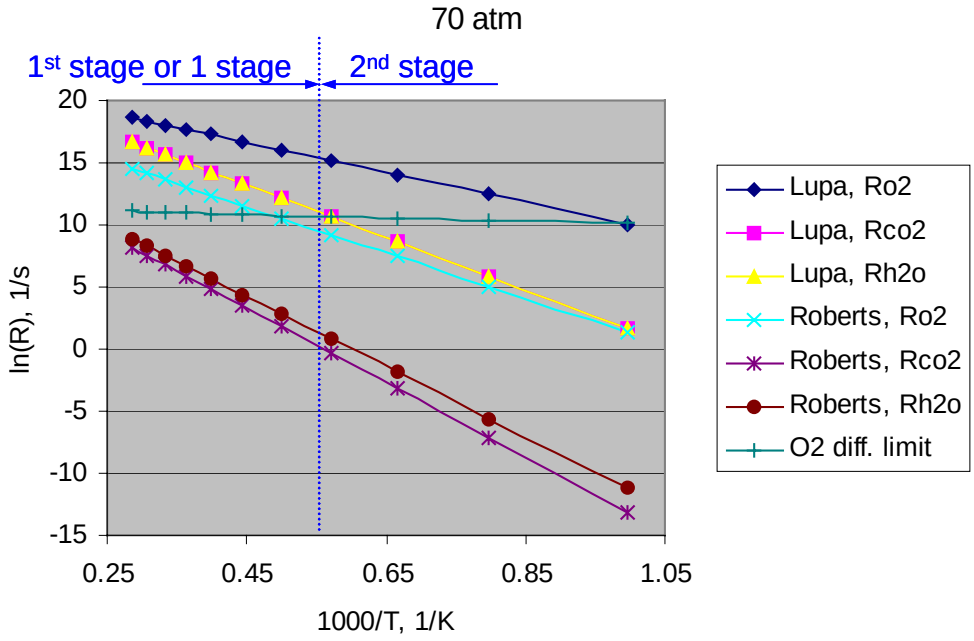


Figure 12. Comparison of the rates at 70 atmospheres from Lupa et al. (1979) and Roberts and Harris (2000) for the apparent reaction rates of $O_2$, $CO_2$, and $H_2O$ (each with a mole fraction of 0.2) with the mass transfer controlled rate for oxygen (also with a mole fraction of 0.2).

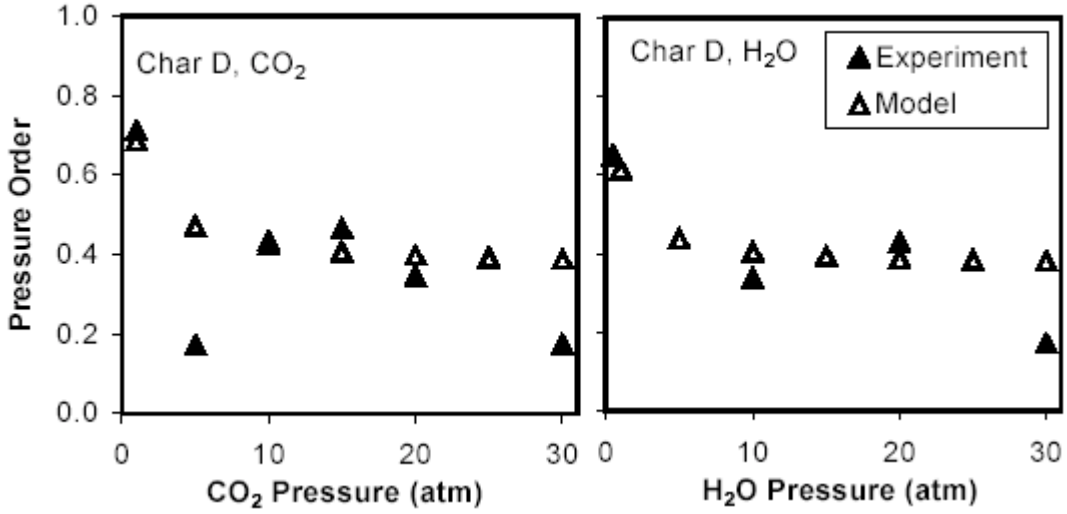


Figure 13. The effect of pressure of gasification gas on the parent order $n_i$ for $CO_2$ and $H_2O$ (Roberts et al., 2001). Comparison of theoretical values (open triangles) with data (closed triangles).

The intrinsic kinetics can be combined with pore diffusion models to obtain the reaction of a particle or derive reactivity per unit external surface area of a particle the so-called apparent reactivity. Data obtained on particles are often correlated in terms of the apparent reactivity. A commonly used correlation used for chemical kinetics is the

$$R_s = k_i P_{si}^{n_i} e^{-E_i/RT} \qquad (25)$$

where the rate constant $k_i$, activation energy $E_i$, and reaction order $n_i$ include the complexity of the internal diffusion and therefore may vary with extent of reaction, and the exponent $n_i$ includes the effects of partial pressures $P_{si}$ of other species at the particle surface and therefore also applies only over a limited range of pressures and gas concentrations. Examples of the dependence of the reaction order on pressure are given for the case of the $H_2O$/carbon and $CO_2$/carbon reactions in Figure 13. The reaction orders $n_i$ are seen to decrease from around 0.7 at one atmosphere to less than 0.2 at 30 atmospheres. The open symbols represent predictions of $n_i$ for $CO_2$ and $H_2O$ based on a model of the saturation of surface sites (Roberts et al., 2001).

The simplified correlation of rate given by equation 25 is the one that has been adopted for the CFD models of a gasifier. The rate parameters can be determined either directly from measurements or from intrinsic reactivities employing a pore model to allow for char structure. The kinetic parameters need to cover the temperatures and oxygen concentrations along different trajectories and will therefore be necessary for environments ranging from nearly pure oxygen near the injector to gasification products (see Table 3 for representative values) near the completion of gasification, temperatures up to 1873 K (2912°F), and pressures of to 8 MPa (~80 atmospheres). In order to calculate the rate, one needs to first obtain the concentration of the reactants at the surface, by equating the rate of diffusion to the surface, by equating $R_D$ from equation 3 to $R_s$ from equation 25 and solving for $P_{si}$, remembering that $C_{si}$ is equal to $P_{si}/RT$.

In order to provide indications of the relative importance of $R_s$ and $R_D$, rates have been calculated for pressures up to 70 atmospheres, and temperatures of 1600 to 3000 K for a single stage gasifier (or first stage of a two-stage gasifier), and down to 1100 to 1300 K for the second stage of a two-stage gasifier. Since the rates can be retarded by combustion products the composition of the residual gases was obtained by assuming that the oxygen entrained flue gases the composition of which was taken from typical values for dry and slurry feed gasifiers (see Table 3).

Table 3. Representative Gasifier Product Composition for Dry and Slurry Feed.

| Component | Dry Coal Feed | $H_2O$ Slurry Feed |
|---|---|---|
| $H_2$ | 26.7% | 30.3% |
| CO | 63.3 | 38.7 |
| $CO_2$ | 1.5 | 10.8 |
| $CH_4$ | 0.0 | 0.1 |
| $H_2S$ | 1.3 | 1.0 |
| $N_2$ | 4.1 | 0.7 |
| Ar | 1.1 | 0.9 |
| $H_2O$ | 2.0 | 16.5 |

The apparent rate $R_s$ is expressed in mass/time of a particle per unit mass and therefore has a dimension of reciprocal time. Values of E, k and n from selected references are shown in Table 4. The literature on char oxidation is enormous and these references were selected because the authors had applied the correlations in the modeling of gasifiers.

Table 4. Selected Kinetics for Char Oxidation with $O_2$

| Authors | E, J/mol | K | n |
|---|---|---|---|
| Banin et al. (1997) | 51048 | 40 kg/(m$^2$·s) | - |
| Joutsenoja et al. (1999) | 82368 | 1903 m/s | 1 |
| Monson et al. (1995) | F($P_t$) | F($P_t$) | 0.5 |
| Lupa and Kliesch (1979) | 100483 | 1404 kg/(m$^2$·s·atm) | 1 |
| Otaka et al. (2001) | 105000* | 95000 1/atm$^n$ | 0.75 |
| Benyon, 2002 | 223000 | $5.81\times10^{10}$- $1.02\times10^{11}$ kg/(m$^2$·s·atm$^n$) | 0.83 |
| Roberts and Harris, 2000 | 153000 | $4\times10^7$ kg/(kg·s·atm$^n$) | 0.85 |

* E in Otaka et al.'s paper is given as 105,000 J/kmol but this gives too small a temperature dependence. The value was interpreted as being J/mol to bring it into line with the other measurements.

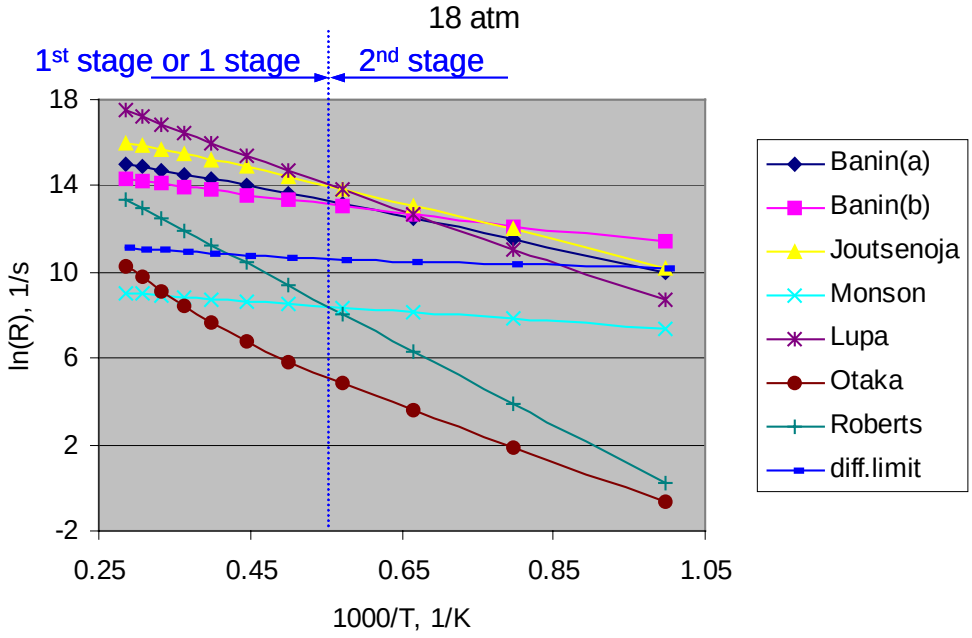


Figure 14. Comparison for a mole fraction of 0.2 oxygen at 18 atmospheres of the apparent kinetic reaction rates from different correlations in the literature with the mass transfer controlled rate.

The importance of a chemical kinetics, $R_s$ calculated from equation 25 with the surface concentration $P_{si}$ equated to the bulk concentration, is compared in Figure 14 with a mass-transfer controlled rate, $R_D$ from equation 23 with $C_{si}$ for the case of reactions at 18 atmospheres with oxygen having a mole fraction of 0.2. There is wide difference in the rates of the different investigators at low temperatures but the data spread is much smaller at the higher temperatures

of interest in the high temperature end. The higher rates, at the temperatures of interest for oxidation in either a single-stage or the first stage of a two-stage gasifier, equal or exceed the mass transfer resistance, with the exception of the results of Monson et al.(1995). As the temperature drops, however, the chemical kinetic rate becomes controlling, underlying the importance of finding good kinetic data on char oxidation.

The rates of gasification with $CO_2$ and $H_2O$ are compared in Figures 11 and 12 with those for gasification with $O_2$ for the kinetics of Lupa and Kliesch (1979) and Roberts and Harris (2000), at total pressures of 18 and 70 atmospheres. The mole fractions of each oxidation or gasification agent were set to 0.2. The kinetics of the reactions with oxygen are greater than those of $CO_2$ and $H_2O$ by a factor of one to three order of magnitude over the temperature range of 800 to 2000 K with the large differences being at the lower temperatures. At the high temperature end of the gasifier the rates of gasification by $CO_2$ and $H_2O$ are therefore approaching that of $O_2$ and can exceed the mass transfer limit. At the low temperatures of the second stage of a two-stage gasifier, the rates of the reactions of gasification with $CO_2$ and $H_2O$ are much smaller than that of $O_2$. Since the $O_2$ concentration in the second stage is small the gasification rate in the second stage will be slow and chemically controlled since the rates shown in Figures 11 and 12 are seen to be lower than the mass transfer limit at the temperature of 1100 to 1350 K, which are typical of the exit temperature of the second stage.

***AIOLOS* Gasifier Module (Transient/Steady State):**

It should be noted that at this time the model development efforts for *AIOLOS* are being performed in a "stand alone" mode, or outside of the workbench. The module for the *AIOLOS* based transient gasifier model will not be implemented into the workbench until after completing all model development and testing on selected transient problems.

During the last performance period, the development efforts for this model have focused on testing the sub-models for coal gasification under high pressure that were implemented into *AIOLOS* in previous performance periods (see Quarterly Progress Report Number 6 for this project). CFD modeling results for a one stage downfired gasifier are described in the Results and Discussion Section at the end of the report (see page 51).

## Task 3.4 Gas Cleanup and other equipment models

In this sub-task we will develop many of the modules required to simulate the Vision 21 energyplex system. This will include models for the:

- Syngas Cooler
- Heat Recovery Steam Generator
- Gas Recuperator
- SCR
- Turbines, compressors and expanders
- Cyclone separator
- Gas Clean Up
- High and Low Pressure Solid Oxide Fuel Cell

These systems will be modeled with 0D or at most 1D reactor models. Many of these models are being created by re-using models developed as part of the LEBS-POC prototype workbench developed during Year One of the program. Details on the models used in the Year One prototype workbench are available in [Bockelie, 2001]. A brief description of the role of each module for the Vision 21 workbench and current model status is described below.

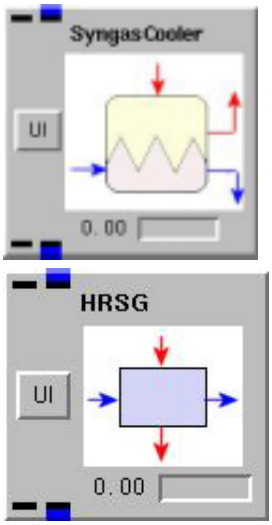


Syngas Cooler and HRSG. Models have been completed for the Syngas Cooler and Heat Recovery Steam Generator (HRSG). These devices are heat transfer equipment used downstream of the gasifier that increases the overall thermal efficiency of the energyplex. The models are 0D models constructed using the steam heat exchanger models developed in the Year One prototype workbench. The steam properties module used in the Year One models has been replaced with a module based on correlations for the ASME 67 steam tables [McClintock and Silvestri, 1970]. The new steam properties module expands the range of temperature and pressure data and includes entropy needed for the steam turbine thermodynamic calculations. The User Interface (UI) includes default inputs to size the Syngas Cooler and HRSG consistent with 118 MWe steam turbine generator output contained in the DOE configuration.

Recuperator. A 0D model has been completed. The recuperator is a gas-to-gas heat exchanger used to preheat the compressed air being fed to the high pressure SOFC. The model is based on the 0D air preheat heat exchanger model developed for the Year One prototype workbench. As per the other heat exchanger models, the recuperator model has been sized for the specified gas temperatures provided by the DOE.

SCR. The data provided by DOE did not include an SCR. Our current SCR model developed in Year One is based on Vanadia/Titania catalysts, which would require placement of the SCR midway in the HRSG for the optimum temperatures. No progress has been made on better defining this model during the last performance period.

Steam Turbines. A simple 0D steam turbine model based on thermodynamic calculations using a user input adiabatic efficiency has been implemented. The efficiency is applied to an isentropic expansion process using the ASME 67 steam properties module.

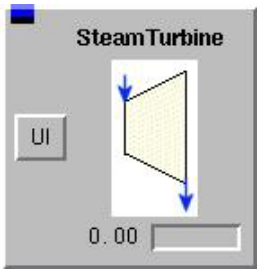


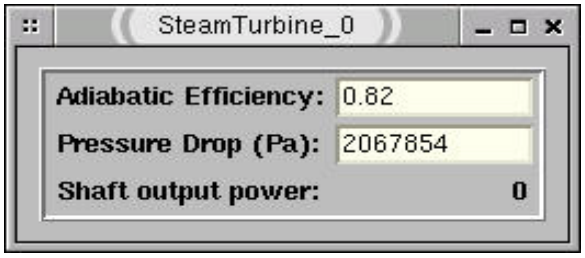


Compressor/Expander: During the last quarter, REI engineers have completed development of simple 0D models for both a compressor and an expander. The same model is used for both components. The thermodynamic calculations involve the assumption of isentropic compression/expansion processes, coupled with user supplied isentropic efficiencies. Other inputs required by the models including species composition, temperature and pressure and provided by the upstream workbench dataflow. Outputs from the models include the exit temperature and power requirements of the device. Modifications of the gas stream passing through the device are transferred to downstream modules by workbench dataflow. Thermodynamic properties needed for these models are obtained using the thermodynamics database class discussed previously.

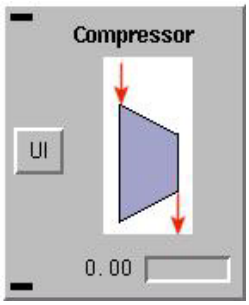


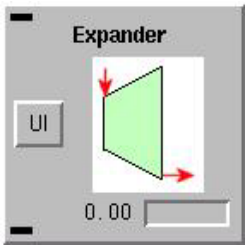


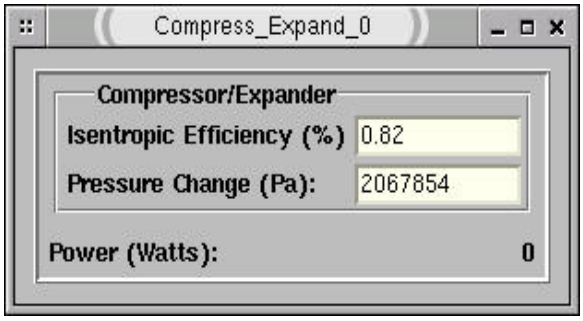


Gas Turbines: With models available for compressors and expanders, we are beginning to focus on the gas turbine combustor. We are currently investigating the possible use of correlation based models as well as a chemical equilibrium based model. If an equilibrium model is employed, it then becomes possible to enhance the model to allow treating the combustor as a continuously stirred reactor with the necessary kinetics calculations.

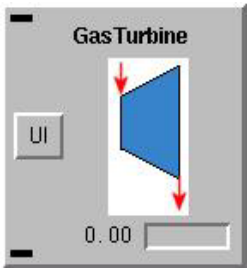

Cyclone Separator: During the past quarter of work, a cyclone separator model has been developed. In the DOE Vision 21 reference configuration the cyclone is located immediately downstream of the gasifier and serves the purpose of eliminating particulate matter from the syngas before it reaches the gas clean up system. This 0D model makes use of mathematical correlations to calculate pressure drop and particulate removal efficiency as a function of particle diameter [De Nevers, 2000]. Model inputs supplied by workbench dataflow include the particle mass flow rate, density and size distribution, gas density and viscosity and mass flow rate. User inputs to the model define cyclone geometry parameters. The model makes use of the thermodynamics database functionality discussed in the previous sections.

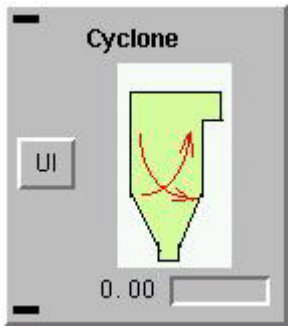


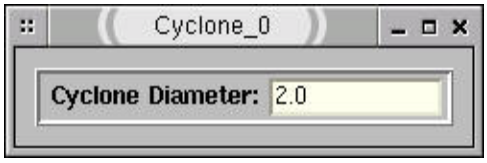


Warm Gas Clean Up. The current generation of gasification systems relies heavily on so-called cold gas clean up systems, which remove particles, acid gases and other trace contaminants at the low temperatures characteristic of conventional power plants and chemical process industry scrubbers. However, DOE has recognized that there is a significant benefit associated with hot gas clean up for gasification systems because of the higher system efficiencies that result when the syngas does not have to be cooled down and reheated before and after the gas clean up process. Several large DOE funded programs have been undertaken to develop hot gas desulfurization systems and hot gas particulate removal systems that would operate at temperatures on the order of 1000 F. Recently, DOE has promoted the use of lower temperatures (500-900 F) for the gas clean up systems, under the umbrella of warm gas clean up systems. Warm gas clean up does not differ in principle from hot gas clean up; at the lower temperatures, new sorbents must be utilized for desulfurization. Such sorbents are currently under development at DOE.


The elements of the gas clean up system can be described in general terms (whether for hot or warm gas clean up). In order to define the system, we assume that the processes that were developed and tested for hot gas clean up can be adapted for warm gas clean up by use of the right sorbents. Figure 15 shows the elements of the warm gas clean up system.

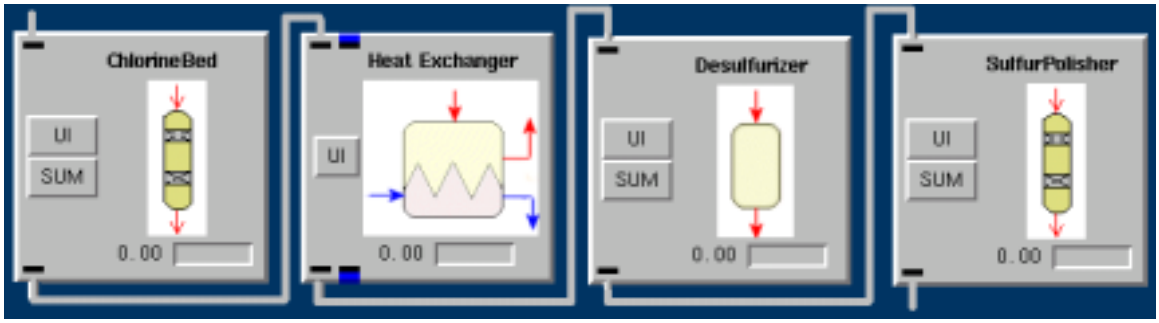


Figure 15. Elements of warm gas clean up system.

During the last performance period, models have been developed for the following components within the warm gas cleanup section:

- chlorine guard bed;
- transport reactor desulfurizer; and
- sulfur polisher.

The units are modeled only how they affect the syngas, without regard to the effects on sorbent or other operational requirements of the equipment. Each gas cleanup unit will, in general, affect the temperature, pressure and composition of the gas. The current models depend heavily on user-specified inputs—only the pressure drop through the system is modeled as the pressure drop directly affects the overall plant efficiency due to the high power costs of gas compression. Currently, the models account for the removal of HCl, $H_2S$, and COS, as these gases are the primary contaminants in the system. The models operate by allowing the user to directly specify the temperature change, the acid gas removal (removal efficiency, or gas exit concentration in ppm), and pressure drop, or use default values supplied. Alternately, the pressure drop can be computed, but is equipment-specific, and requires specific user-inputs as discussed below. Figure 16 shows the user interface for the chlorine bed module, which is similar to the transport reactor desulfurizer and the sulfur polisher.

The gas temperature is expected to change across each of the units due to heat losses to the environment, and to a lesser extent, heats of reaction as the acidic gaseous species are adsorbed. These temperature changes are expected to be small compared to the overall gas temperature and represent a tiny fraction of the overall plant power output. In addition, while temperature changes are small, variations in the temperature change with specific operating conditions are even smaller. Consequently, the user specifies the temperature change in a unit directly, or can use a default value supplied.

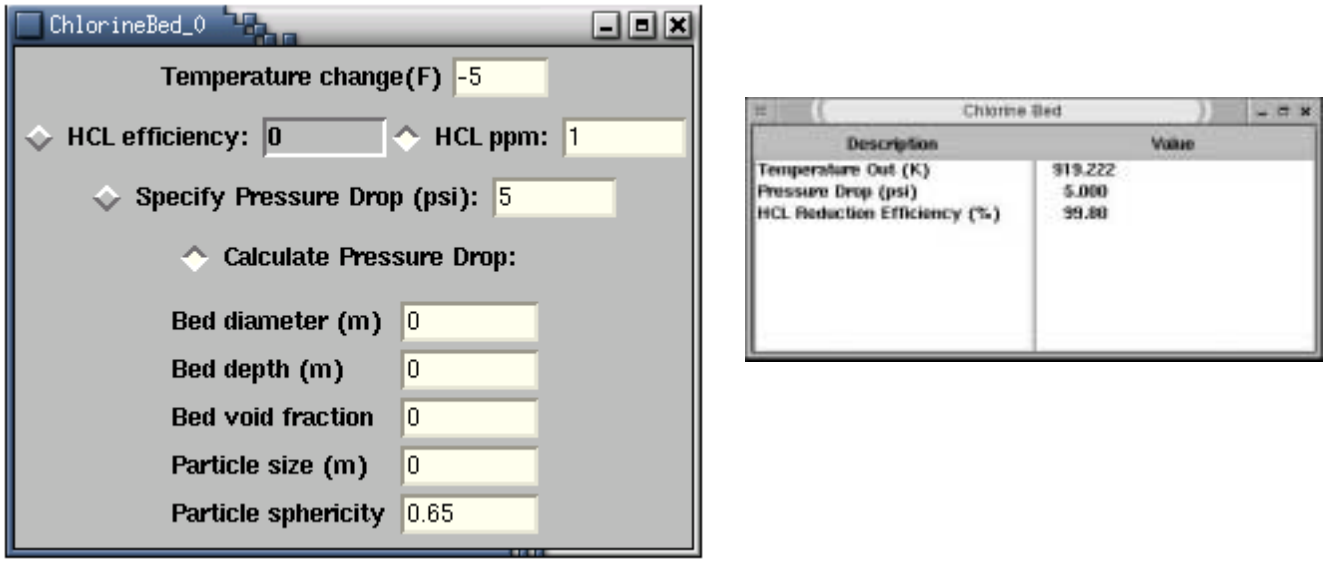


Figure 16. User interface for the chlorine bed module.

Due to the lack of full-scale operating experience with warm gas cleanup systems and incomplete sorbent properties, kinetics, etc., the acid gas species are simply removed from the units by allowing the user to specify either removal efficiencies, or exit concentrations in ppm. The chlorine bed allows for the removal of HCl only, while the transport reactor and sulfur polisher allow removal of both $H_2S$ and COS. As for the temperature and pressure drop, default values are provided.

The default values provided for temperature changes and pressure drop are taken as estimated values based on a combination of information from Figure 2 and process flow sheet data from a DOE-NETL funded analysis of various cold and hot gas clean-up systems for an IGCC plant with a Texaco-style gasifier [Shelton and Lyons, 2000]. The default values for acid gas species removals are taken from typical values expected for the given units as required for the downstream equipment, as listed in Table 5. Listed in Table 6 is a summary of the default values provided in our models.

Table 5. Sulfur Removal Requirements for Syngas Applications

| Application | Total Sulfur ($H_2S$ + COS), ppmv | $H_2S$ Alone, ppmv |
|---|---|---|
| Gas Turbine | <20 | Not specified |
| Molten Carbonate Fuel Cell (MCFC) | 0.5 | Not specified |
| Phosphoric Acid Fuel Cell (PAFC) | <50 | <20 |
| Solid Oxide Fuel Cell (SOFC) | <0.1 | Not specified |
| Chemical production | <0.06 | |

Table 6. Summary of default values for gas cleanup units. Values are estimated.

| | Pressure Drop (psi) | Temperature Change ($^oF$) | HCl Concentration (ppm) | $H_2S$ Concentration (ppm) | COS Concentration (ppm) |
|---|---|---|---|---|---|
| Chlorine Bed | 15 | -5 | 1 | --- | --- |
| Transport Reactor | 10 | 10 | --- | 10 | 1 |
| Sulfur Polisher | 5 | 0 | --- | 0.1 | 0.01 |

The pressure drop in each of the three units can be modeled if the user has specific equipment specifications. The chlorine bed and sulfur polisher are fixed bed units. The pressure drop is modeled through each of these units in the same way and is based on the Ergun equation [Kunii and Levenspiel, 1969]:

$$\frac{\Delta P}{L} = 150 \cdot \frac{(1-\varepsilon)^2}{\varepsilon^3} \cdot \frac{\mu \cdot u_o}{(\phi \cdot d)^2} + 1.75 \cdot \frac{(1-\varepsilon)}{\varepsilon^3} \cdot \frac{\rho \cdot u_o^{\,2}}{\phi \cdot d}, \qquad (26)$$

where P is the pressure, L is the bed depth, ε is the bed void fraction, d is the sorbent particle diameter, ϕ is the particle sphericity, μ is the gas viscosity, ρ is the gas density, and $u_o$ is the gas superficial velocity. To apply this equation, the user must specify the bed depth, particle diameter and sphericity, bed void fraction, and the bed diameter (to compute the gas superficial velocity.) The gas viscosity and density are computed as a function of temperature and composition. A typical default value of 0.65 is provided for the particle sphericity. The bed void fraction depends on the packing particle size, and shape, and the method of packing. A plot of void fraction versus particle sphericity is given by Kunii and Levenspiel, as cited above. The pressure drop is computed neglecting wall friction and static head losses, as they are expected to be much smaller than the pressure drop through the packed bed.

The transport reactor desulfurizer operates with the sorbent particles carried co-currently with the gas stream. The void fraction in these units is generally fairly large. The pressure drop is again correlated by the Ergun equation with additional terms to account for the static head pressure drop (pressure loss in suspending the solid particles,) and the wall friction. The following equation is used [Wen and Galli 1971]:

$$\frac{\Delta P}{L} = \frac{150 \cdot \mu \cdot (1-\varepsilon)^2 \cdot (u_o/\varepsilon - u_p)}{(\varepsilon \cdot \phi \cdot d)^2} + \frac{1.75 \cdot (1-\varepsilon) \cdot \rho \cdot (u_o/\varepsilon - u_p)^2}{\varepsilon \cdot \phi \cdot d} + (1-\varepsilon) \cdot (\rho_s - \rho) \cdot g + \frac{\rho \cdot u_o{}^2 \cdot f}{2 \cdot D \cdot \varepsilon^2}, \quad (27)$$

where all variables are defined above, and $\rho_s$ is the particle density, D is the unit diameter, $u_p$ is the particle velocity, g is the gravitational acceleration, and f is the Fanning friction factor. In this equation, the first two terms account for the fluid/particle friction losses, the third term is the static head loss, and the last term is the wall friction loss. The wall friction term ignores the effect of the particles. The fanning friction factor for rough pipes is used [Perry, 1997],

$$f = \left[ -4 \cdot \log\left( \frac{0.27 \cdot \varepsilon}{D} + (7/\mathrm{Re})^{0.9} \right) \right]^{-2}, \quad (28)$$

where Re is the Reynolds number, and ε is the wall roughness, taken as 0.05 mm. The user is required to specify the sorbent particle density, or use a default value of 2 g/cm$^3$. The mass throughput of sorbent is also required, to compute the sorbent particle velocity from the following material balance equation, where G is the solids mass flow rate:

$$u_p = \frac{4 \cdot G}{\pi \cdot D^2 \cdot \rho_s \cdot (1-\varepsilon)}. \quad (29)$$

The output of each gas cleanup model includes the gas temperature, pressure, and acid gas species removal efficiency; the overall stream composition is also available.

The development effort for the chlorine bed guard, desulfurizer, sulfur polisher models described above is complete.

For future reference, shown below is the User Interface for the bed-desulfurizer and sulfur polisher. Also shown are example outputs from these models.

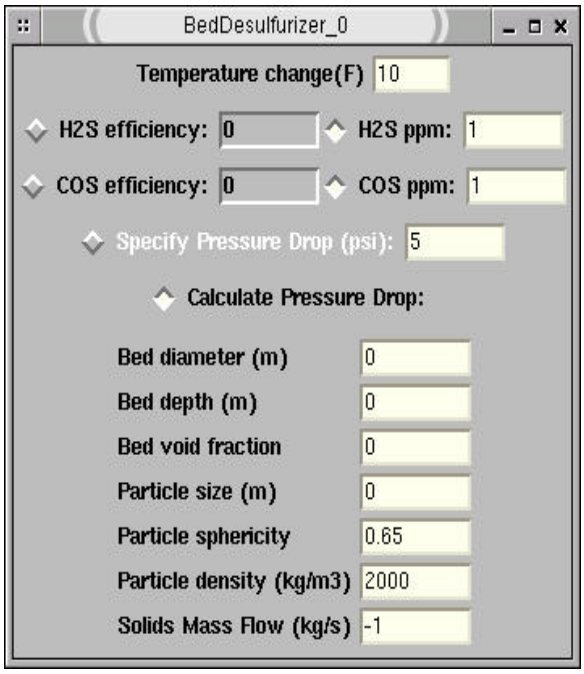


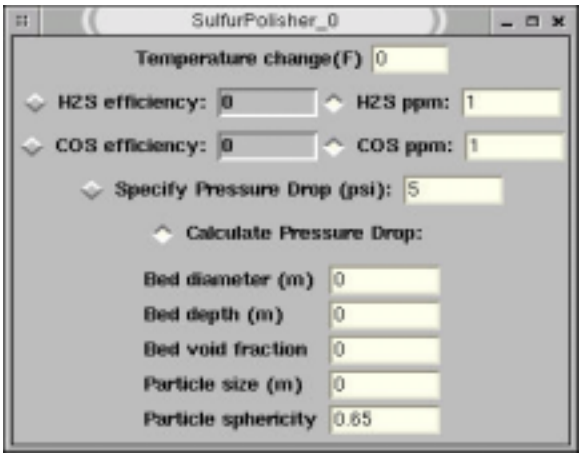


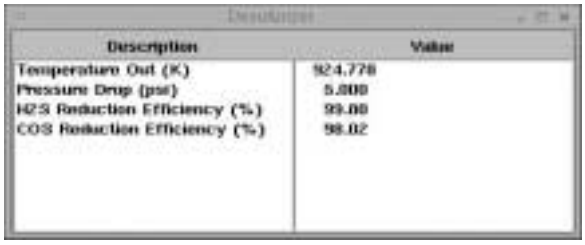


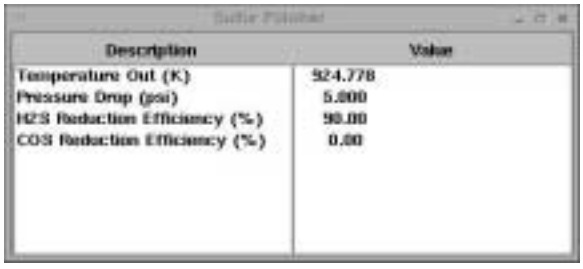


<u>High and Low Pressure Solid Oxide Fuel Cells</u>. We plan to include simple reactor models for the high pressure (HP) and low pressure (LP) Solid Oxide Fuel Cell (SOFC). The models will be 0D (or possibly 1D), mass energy balance models for simple configurations that exhibit the important fluid dynamics, heat transfer, chemical and electrochemical reactions, species transport, etc. The SOFC models will provide a simple test platform to understand the gross effects for SOFC cells. Preliminary discussions have been held with the National Fuel Cell Research Center (NFCRC) at the University of California, Irvine. In addition, preliminary discussions have been held with the DOE to pursue the possibility of including 0D and 1D SOFC models that have developed at the DOE-NETL.

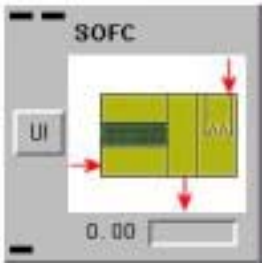

# Results and Discussion

During the last quarter we have placed a heavy emphasis on developing CFD models for the entrained flow gasifier models. Described below are preliminary CFD modeling results.

## *GLACIER* Gasifier Model

In this section we describe a series of CFD simulations that have been performed with the gasifier model for the one stage (downfired) and two stage (upfired) "generic" gasifier designs. In this work we do not attempt to optimize the design or operation of a gasifier. Rather, our objective is to exercise the model in order to develop a basis for addressing questions on the reliability of the predicted values and the sensitivity of the model to important model and operational parameters even though these may fall outside the region of practical operating conditions. Simulations targeted toward improving gasifier operation and design will be performed at a later date.

For comparing the predicted gasifier performance we focus on characteristics of the syngas generated, in addition to the basic flow field features. The principle items of interest are the carbon conversion (i.e., % of carbon from the solid fuel converted to carbon in the syngas) and the syngas temperature, composition, higher heating value (HHV, BTU and BTU/SCF) and cold gas efficiency (CGE) which is defined as [Benyon et al, 2000]:

$$CGE = (\dot{M}_{syngas} * HHV_{syngas}) / (\dot{M}_{fuel} * HHV_{fuel}) \qquad (30)$$

where $\dot{M}_{fuel}$ and $\dot{M}_{syngas}$ are the mass flow rate of the fuel and syngas, respectively, and $HHV_{fuel}$ and $HHV_{syngas}$ are the higher heating value of the fuel and syngas, respectively.

In the following section we discuss, in order, the geometry of the two gasifiers used in this study, the baseline operating conditions, simulation results for the baseline conditions and then a series of parametric simulations that have been performed to evaluate the impact on predicted performance for varying fuel grind, slurry pre-heat, wet and dry fuel feed, system pressure, reaction kinetics, fuel type and gasifier length. Due to complications with implementing the slagging wall model into the CFD code, most of the simulations described below were performed assuming an adiabatic wall boundary condition.

### Gasifier Geometry

In general, the internal dimensions of commercial gasifier designs are proprietary information. Hence, the geometry of the gasifiers used in this study are based on a combination of publicly available information (e.g., conference papers, advertising literature, web pages, etc.) and engineering judgment.

The internal shape of the single stage gasifier is based on information for a pilot scale facility [Schneyer et al., 1982] and then scaled for commercial scale systems. For the single stage gasifier (see Figure 14), we assume a L/D ratio of two, where L is the length of the main chamber and D is the internal diameter to the refractory surface. Based on simple plug flow calculations, this results in a gas residence time for the gasifier of about one half of one second. The single stage gasifier contains a single nozzle positioned at the top, center of the reactor through which the oxidant stream and coal-water slurry mixture are injected into the gasifier. The injector is assumed to be an annular nozzle with the oxidant stream passing down a center

passage, a slipstream of steam and the slurry is located in an annular passage a small distance from injector centerline. The slurry stream is oriented toward the injector centerline (at the injector tip) that results in a spray entering the gasifier. At the point where injector exhausts into the gasifier chamber, we assume the coal-water slurry is traveling at about 60 m/s and the oxidant stream is assumed to have a radial profile that has an average velocity of about 100 m/s.

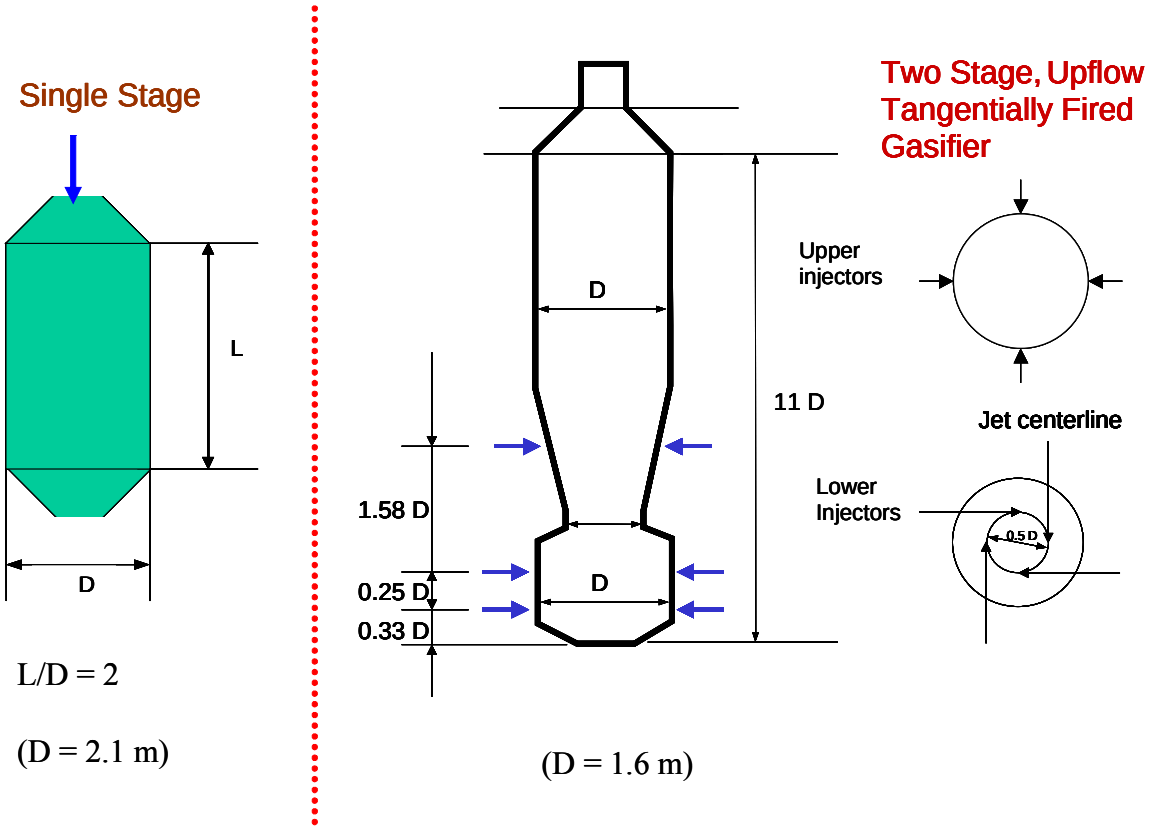


Figure 16. One stage and two stage gasifier geometries.

The shape of the two stage gasifier (see Figure 14) is based on information contained in a series of articles by Chen et al. [Chen et al., 1999], [Chen et al., 2000] that describe modeling studies and scale-up for a pressurized, air blown entrained flow gasifier designed to operate at 2000 tons per day of coal. Additional assumptions used to determine the size of the gasifier were that the gasifier should provide about a two second residence time for the gases (assuming idealized flow) and has a length to diameter ratio (L/D) of about ten. For the two stage gasifier, the length L is based only on the vertical riser section (of constant diameter) and D is the internal diameter of the riser; for the dimensions of the combustion chamber at the bottom of the gasifier engineering judgment was utilized to scale the size information contained in the articles by Chen et al. The two stage gasifier contains three levels of symmetrically placed injectors. The fuel injectors are assumed to have a simple annular passage (concentric pipes) that do not produce a spray action. The bottom two levels of injectors are oriented as per a tangential firing system to

create a strong swirling flow field that spirals upward along the axis of the gasifier. The upper level of injectors are oriented opposed to each other.

Baseline Conditions

The baseline operating conditions are taken from a Vision 21 IGCC reference configuration provided by the DOE to Reaction Engineering International for use in our DOE Vision 21 project. For simplicity, the configuration is shown again in Figure 17. The IGCC reference configuration consists of an entrained flow gasifier, gas clean up system, gas turbines, heat recovery steam generator, steam turbine and SOFC fuel cells.

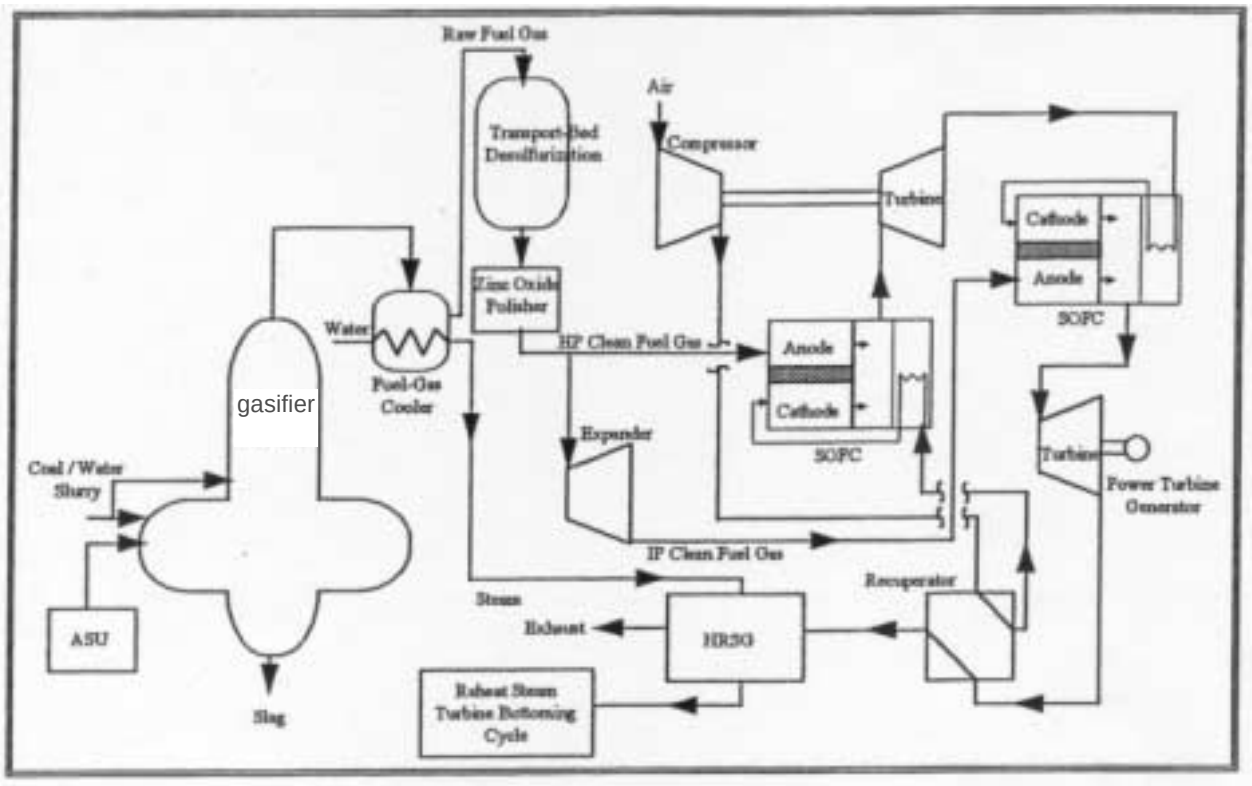


Figure 17. Vision 21 IGCC reference configuration.

Although the reference configuration is based on a two-stage gasifier, we have used the same baseline conditions for testing both classes of gasifier. The key parameters with respect to the gasifier are 3000 tons/day of Illinois #6 coal (see Table 2 above or Table 7 below which contains information on the coals used in the parametric study). For the most of the simulations, we use the kinetic parameters in [Lupa and Kliesh, 1979] which have been derived for Illinois #6 across a range of temperatures and pressures that are representative of gasifier conditions. The system pressure for the gasifier is set at 18atm. The coal-water slurry is 74% solids by weight and the slurry temperature is assumed to be 422 K, or slightly less than boiling at the baseline system pressure. The oxidant stream is assumed to be 95% $O_2$ and 5% $N_2$ and to enter the gasifier at a temperature of 475 K. For the two stage gasifier, 78% of the coal and all of the oxidant is uniformly distributed amongst the fuel injectors in the first stage and the remaining coal is uniformly across the injectors in the second stage. Note that there is no oxidant injected into the upper stage. The overall oxygen:carbon ($O_2$:C) mole ratio is ~0.40, resulting in an overall

stoichiomery of about 0.47 and a stoichiometry in the lower stage of about 0.60. A one stage gasifier is typically run at a slightly higher oxidant:carbon mole ratio than is a two stage gasifier. Hence, the baseline simulation has been performed with an oxygen:carbon ratio of 0.50, resulting in an inlet stoichiometry of about 0.54. The operating conditions used in this project are very close to the conditions used for the "Hot Gas Cleanup" Aspen simulations contained in [DOE-NETL, 2000a] and [DOE-NETL, 2000b].

Table 7. Fuel properties used for this study

| | Illinois #6 | Petcoke | PRB coal |
|---|---|---|---|
| Proximate Analysis | As-Received (wt%) | As-Received (wt%) | As-Received (wt%) |
| Moisture | 11.12 | 7.00 | 29.00 |
| Ash | 9.70 | 0.52 | 4.82 |
| Volatile Matter | 34.99 | 12.36 | 31.38 |
| Fixed Carbon | 44.19 | 80.12 | 34.80 |
| TOTAL | 100.00 | 100.00 | 100.00 |
| HHV (Btu/lb) | 11666 | 14282 | 8618 |
| Ultimate Analysis | As-Received (wt%) | As-Received (wt%) | As-Received (wt%) |
| Moisture | 11.12 | 7.00 | 29.00 |
| Carbon | 63.75 | 81.37 | 50.73 |
| Hydrogen | 4.50 | 2.55 | 4.23 |
| Nitrogen | 1.25 | 0.92 | 0.86 |
| Sulfur | 0.29 | 4.81 | 0.31 |
| Ash | 9.70 | 0.48 | 4.82 |
| Oxygen (by difference) | 6.88 | 2.87 | 10.05 |
| TOTAL | 100.00 | 100.00 | 100.00 |

Baseline Simulations

One Stage Configuration

Illustrated in Figure 18 is the gross flow field for the one stage gasifier for baseline firing conditions. Shown in Figure 18a is the predicted gas temperature at selected elevations and representative coal particle trajectories, colored by coal volatile content. Illustrated in Figure 18b is the axial velocity at selected elevations and representative coal particle trajectories, colored by coal char content. Overall, the flow field is similar to that of an immersed jet exhausting into a confined volume. There is a core of high velocity, hot gas traveling down the center of the gasifier. Away from the centerline, there exists a slow moving, much cooler reversed flow (i.e., recirculating flow) that travels back toward the injector end of the gasifier. From the particle trajectories it can be seen that the fuel enters the chamber and quickly devolatilizes. Likewise, the fuel initially contains no char, rapidly forms char and then burns out (oxidizes) the char through the remainder of the chamber.

Illustrated in Figure 19 are XY plots showing the gas temperature along the axis of the gasifier. Shown in the temperature plot are the bulk gas temperature, centerline gas temperature, average gas temperature near the wall surface and the average temperature at the wall (or slag) surface. The bulk temperature plot shows a peak value very near the injector, indicating that a large amount of the fuel ignites very soon after entering the gasifier. The peak gas temperature along

the chamber centerline does not occur until about one-third of the distance down the gasifier due to the fuel not being the center stream in the fuel injector. The drop in temperature further into the gasifier is due to the endothermic reactions in the gasification reactions. Comparison of the gas temperature near the wall to the bulk and centerline temperatures emphasizes the severe gradients in the temperature field in the radial direction. In contrast, note that the plots of the near wall gas temperature and wall surface temperature show only a modest change in value along the length of the gasifier.

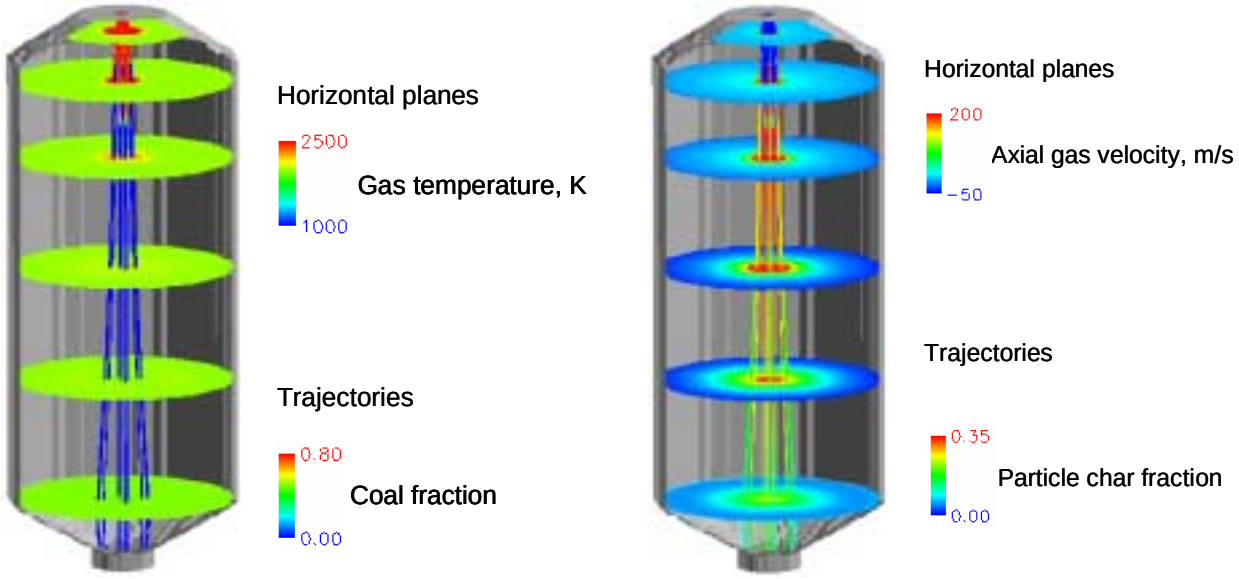


Figure 18. One stage gasifier. (a) Gas temperature and fuel particle coal fraction (left). (b) Gas temperature and fuel particle char fraction.

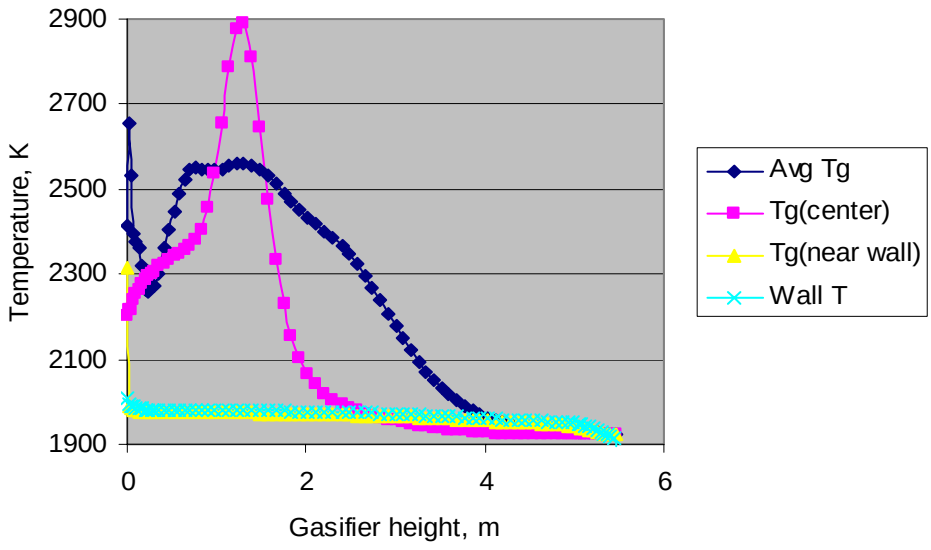


Figure 19. One stage gasifier. Plotted as a function of axial position are the average gas temperature, centerline gas temperature, average gas temperature near the wall and the average wall temperature.

Illustrated in Figure 20a are XY plots for the gas composition along the gasifier axis. The plots show a rapid raise in CO and $H_2O$ content, with the $H_2O$ achieving a peak value at about one-third of the distance down the gasifier, after which both the $H_2O$ and $CO_2$ content decrease due to the gasification reactions. Shown in Figure 20b are plots of the bulk, centerline and near wall concentration of $H_2$. Due to the fuel injector configuration, there is no significant $H_2$ concentration until about one-third of the distance down the gasifier, near where the centerline gas temperature reached a peak value. In contrast, the bulk $H_2$ concentration shows a very rapid rise in value within a short distance of the injector. Note that the average $H_2$ concentration near the wall shows almost a constant value throughout the gasifier. Last, all three plots converge to the same value by about two-thirds of the way through the gasifier.

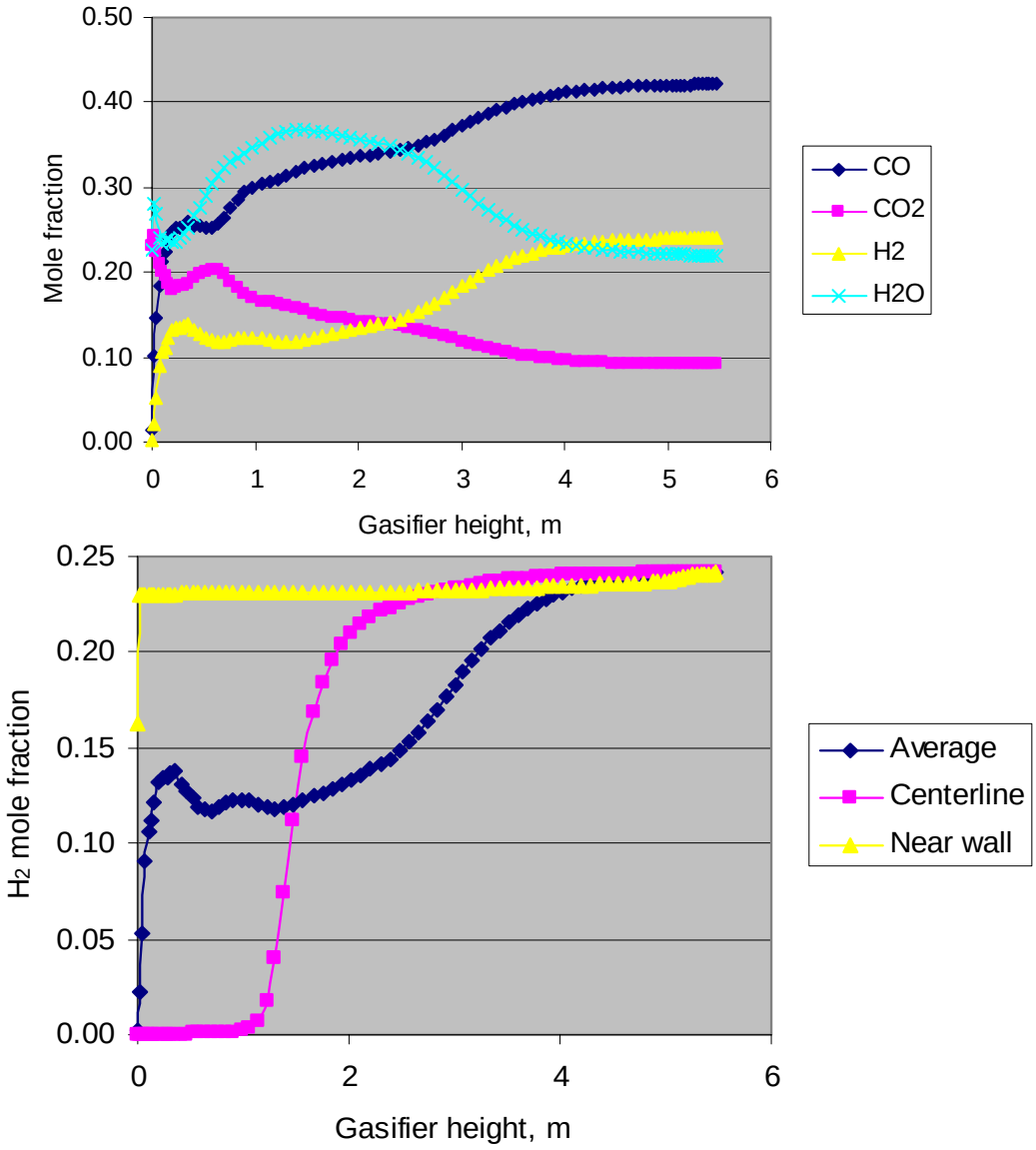


Figure 20. One stage gasifier. Plotted as a function of axial position are (top - a) average concentration of major gas species and (bottom - b) average, centerline and near wall concentration of $H_2$.

Shown in Table 8 are the average values for the syngas quantity and composition at the gasifier exit. For plant operations the syngas conditions are typically reported on a dry basis for measurements taken at a location downstream of the syngas clean-up system. For simplicity, our results are reported on a wet basis at the model exit plane. From the table it can be seen that for the baseline conditions the model predicts a high carbon conversion (over 97%), cold gas efficiency of slightly more than 75% and a syngas heating value of about 224 Btu/SCF. A DOE funded study that employed an ASPEN analysis for an IGCC plant with a single stage gasifier [DOE-NETL, 2000a] predicted a normalized higher heating value of 240 Btu/SCF for comparable operating conditions (same coal and slurry flow rate, lower oxidant flow rate, higher gasifier pressure) to those used in this simulation.

Listed in the table are some reference values for gas, solid and droplet residence times. The Plug Flow Reactor (PFR) residence time provides a reference for the gas residence time and is computed from a single, volume averaged gas density for the reactor and assuming a plug flow; for the given conditions and reactor volume this results in a PFR residence time of about 0.6 seconds. Due to the strong re-circulating flow pattern within the gasifier chamber one must be careful of what is concluded based on the PFR residence. For fuel particles, the model predicts an average residence time of slightly less than 0.03 seconds. For particles, the residence time is defined as the time from when the particle enters the reactor until it impacts on a wall or exits the gasifier. Note that even if the particle "burns out", we continue to track the remaining ash particles until the ash impacts the wall or exits the gasifier. Considering the high velocity flow passing down the center of the gasifier (see Figure 18b), the short residence time of the particles is not unreasonable. For this case, the average residence time for slurry water droplets (i.e., the average time required for a water droplet to evaporate) is about one fifth the residence time of the fuel particles. For many of the parametric simulations that have been performed the droplet residence time changes only slightly where as the residence time of the fuel particles can change significantly.

Table 8. One Stage Gasifier Baseline

| | |
|---|---|
| Exit Temperature, K | 1922.7 |
| Carbon Conversion, % | 97.15 |
| Exit LOI, % | 18.86 |
| PFR Residence Time, s | 0.653 |
| Particle Residence Time, s | 0.026 |
| Mole Fraction: CO | 0.4217 |
| $H_2$ | 0.2413 |
| $H_2O$ | 0.2192 |
| $CO_2$ | 0.0910 |
| $H_2S$ | 0.0079 |
| COS | 0.0005 |
| $N_2$ | 0.0182 |
| Exit Mass Flow, klb/hr | 542.09 |
| HHV of Syngas, Btu/lb | 4139.4 |
| HHV of Syngas, Btu/SCF | 223.7 |

Two Stage Configuration

Illustrated in Figure 21 is the gross flow field for the two stage gasifier for baseline operating conditions. To simplify plotting, only the bottom half of the gasifier is included in the figure. Shown in Figure 21a is the predicted gas temperature at selected elevations and representative coal particle trajectories, colored by coal volatile content. Illustrated in Figure 21b is the CO content at selected elevations and representative coal particle trajectories, colored by coal char content. From the figures one can see a strong, swirling flow pattern in the gas flow and the particle trajectories in the lower section. This pattern is to be expected with a tangential firing system used for the lower injectors. Looking at the flow field immediately in front of the top level of injectors the flow pattern changes due to these injectors being oriented opposed to each other. As illustrated by the fuel particle trajectories shown in Figure 21a, the fuel injected into the first stage devolatilizes very quickly but the fuel injected at the top injectors requires a slightly longer time to devolatilize. The char from fuel injected in the first stage gasifies prior to reaching the upper injectors. However, the char in the fuel particles from the upper injectors requires a very long time to fully gasify.

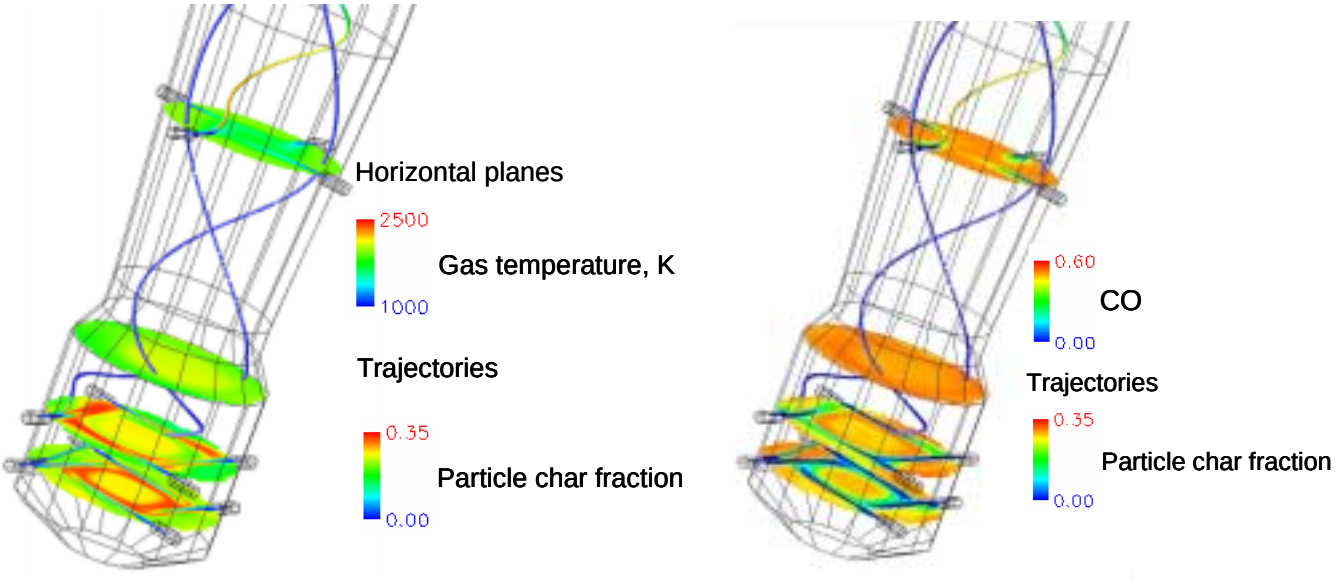


Figure 21. Two stage gasifier. (a) Gas temperature and fuel particle coal fraction (left). (b) CO concentration and fuel particle char fraction.

Illustrated in Figure 22 are XY plots showing the gas temperature along the axis of the gasifier. Shown are the bulk gas temperature, centerline gas temperature, average gas temperature near the wall surface and the average temperature at the wall (or slag) surface. The XY plots are started at 1 m because the complex swirling flow at the very bottom of the gasifier does not allow computing a sensible average value. All of the values show a sharp change in value at about the 4 m elevation where the upper injectors are located. At about the 11 m level (60% of the gasifier height), all of the values converge. Note that in the first stage, the centerline temperature is greater than the near wall gas temperature, but above the top injector the centerline temperature drops well below the near wall temperature. The overall decrease in gas temperature through the chamber is due to the endothermic reactions associated with gasification.

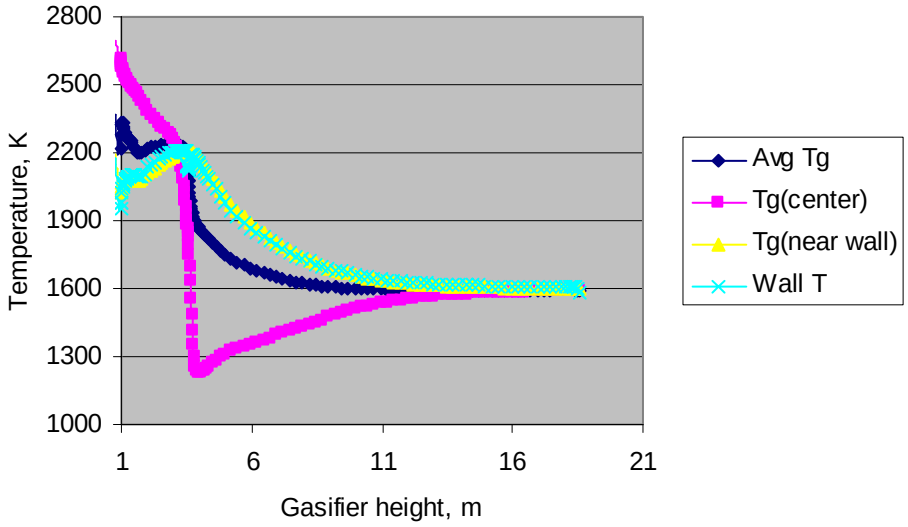


Figure 22. Two stage gasifier. Plotted as a function of axial position are the average gas temperature, centerline gas temperature, average gas temperature near the wall and the average wall temperature.

Illustrated in Figure 23 are XY plots for the gas composition along the gasifier axis. The plots indicate little change in the major species concentrations (on average) for the region between the top of the second level of injectors to just below the upper injectors. At the upper injectors the average composition shows a relatively sharp change for a short distance after which the values asymptote to their final values. There is little if any change in moisture concentration after the 12 m elevation, implying that little gasification occurs above this level. Comparing the plots of bulk, centerline and near-wall $H_2$ gas concentration it can be seen that in the lower 50% of the gasifier, the local gas concentration exhibits more variations in value along the length of the gasifier than are observed by only looking at the bulk value.

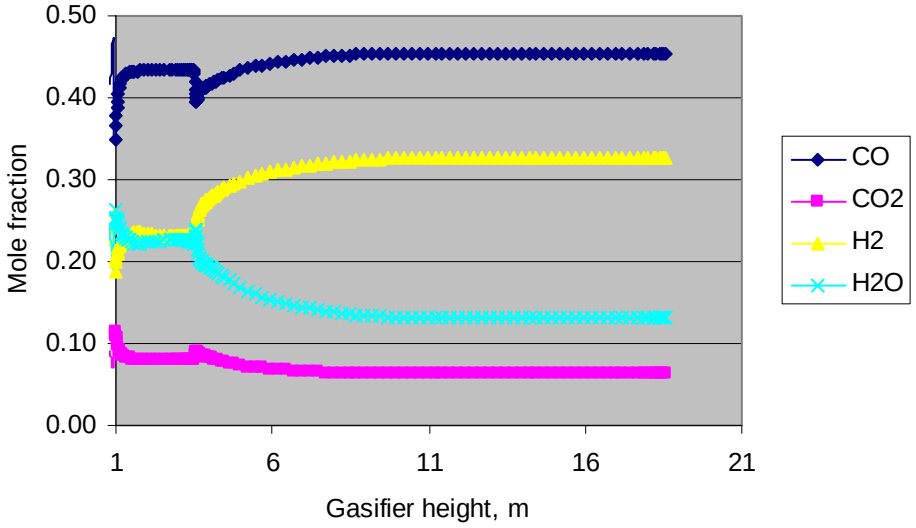


Figure 23a. Two stage gasifier. Plotted as a function of axial position are average concentration of major gas species.

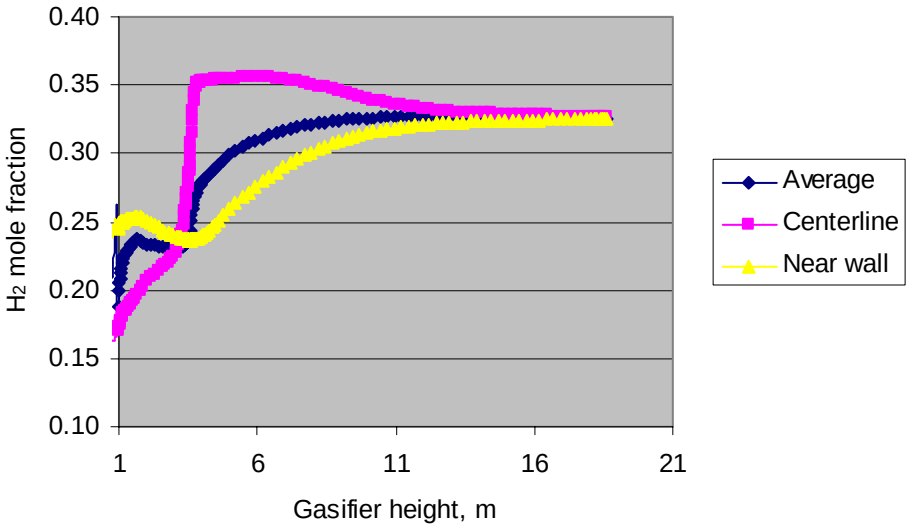


Figure 23b. One stage gasifier. Plotted as a function of axial position are average, centerline and near wall concentration of $H_2$.

Shown in Table 9 are the average values for the syngas quantity and composition at the gasifier exit. From the table it can be seen that for the baseline conditions the model predicts a high carbon conversion (over 99%), cold gas efficiency of slightly more than 87% and a syngas heating value of about 257 Btu/SCF. These values are much higher than that predicted for the single stage gasifier. A DOE funded study that employed an ASPEN analysis for an IGCC plant with a single stage gasifier [DOE-NETL, 2000b] predicted a normalized higher heating value of 250 Btu/SCF for comparable operating conditions as used in this simulation (same coal, slurry and oxidant flow rate, higher gasifier pressure and use flue gas recycle to temper exit temperature). Listed in the table are values for the residence times of the gas and fuel particles. For the given conditions and reactor volume this results in a PFR residence time of about 1.5 seconds. For fuel particles, the model predicts an average residence time of slightly less than one second. The strong swirling flow pattern provides the means to greatly increase the fuel residence time.

Table 9. Two Stage Gasifier Baseline

| | |
|---|---|
| Exit Temperature, K | 1594.9 |
| Carbon Conversion, % | 99.32 |
| Exit LOI, % | 1.48 |
| PFR Residence Time, s | 1.520 |
| Particle Residence Time, s | 0.996 |
| Mole Fraction: CO | 0.4541 |
| $H_2$ | 0.3259 |
| $H_2O$ | 0.1324 |
| $CO_2$ | 0.0630 |
| $H_2S$ | 0.0081 |
| COS | 0.0004 |
| $N_2$ | 0.0154 |
| Exit Mass Flow, klb/hr | 502.18 |
| HHV of Syngas, Btu/lb | 5195.8 |
| HHV of Syngas, Btu/SCF | 257.2 |
| Cold-Gas Efficiency, % | 87.3 |

In the following we present numerical results for parametric studies that have been performed with the model. In general, there is relatively little visible change in plots of the gasifier flow field for the parametric cases. Hence, we present only tabulated values.

Effect of Average Fuel Particle Size

Fuel particle size is an important parameter for gasifier unit operation. In general, for coal combustion/gasification a finer grind (i.e., smaller mass mean particle size) reduces the time for combustion or gasification to occur. Hence for a fixed reactor chamber, more fuel conversion will occur. From a design viewpoint, the reduced time for fuel conversion would allow using a smaller (shorter) reactor and thereby potentially reduce cost. Pulverized coal is typically generated with a mill that uses parasitic power to operate. The finer the grind, the greater the parasitic power needs. Hence there is a trade-off that plant designer/operators must consider. Regardless of the fuel grind for which the gasifier is originally configured, particle size can (will) vary over time due to wear-and-tear on mills, equipment outages, etc.

Listed in Table 10 is a summary of the predicted gasifier performance for varying the fuel grind in the one stage gasifier. The three particle sizes modeled are mass mean particle sizes of 30, 40 and 60 microns, or 96%, 90% and 72% through 200 mesh, respectively. The assumption of a mass mean particle size of 40 microns for the baseline simulation is based on information from [Chen et al, 1999], [Chen et al, 2000]. As expected, the model predicts that increasing the average particle size decreases the carbon conversion, which results in an increase in exit gas temperature and lower heating value and cold gas efficiency. The increase in gas temperature is due to the sub-stoichiometric (fuel rich) conditions – that is less carbon conversion results in an oxygen fuel mixture that is slightly closer to stoichiometric and thus slightly hotter. The unburned carbon in the flyash (LOI) increases with increasing particle size. Although the different particle sizes resulted in about a 1% change in the syngas heating value, this change would be hard to identify by looking only at the syngas composition, which is quite similar for all three cases. Also listed in Table 10 is a summary of the predicted gasifier performance for varying the fuel grind for the two-stage gasifier. The model predicts a very slight decrease in carbon conversion, heating value and cold gas efficiency. Although the expected trend is captured, the changes in values are almost too small to be reliable.

Table 10. Effect of Particle Size

| | One Stage | | | Two Stage | | |
|---|---|---|---|---|---|---|
| Particle Size, μm | 30.0 | 40.0 | 60.0 | 30.0 | 39.8 | 60.0 |
| Exit Temperature, K | 1889.0 | 1922.7 | 1953.6 | 1592.5 | 1594.9 | 1616.2 |
| Carbon Conversion, % | 97.91 | 97.15 | 95.63 | 99.45 | 99.32 | 98.78 |
| Exit LOI, % | 14.56 | 18.86 | 26.32 | 3.31 | 1.48 | 0.30 |
| PFR Residence Time, s | 0.661 | 0.653 | 0.635 | 1.523 | 1.520 | 1.505 |
| Particle Resdience Time, s | 0.919 | 0.996 | 0.027 | 0.919 | 0.996 | 1.037 |
| Mole Fraction: CO | 0.4232 | 0.4217 | 0.4170 | 0.4542 | 0.4541 | 0.4532 |
| $H_2$ | 0.2452 | 0.2413 | 0.2350 | 0.3262 | 0.3259 | 0.3234 |
| $H_2O$ | 0.2143 | 0.2192 | 0.2275 | 0.1320 | 0.1324 | 0.1357 |
| $CO_2$ | 0.0905 | 0.0910 | 0.0935 | 0.0630 | 0.0630 | 0.0631 |
| $H_2S$ | 0.0079 | 0.0079 | 0.0078 | 0.0081 | 0.0081 | 0.0081 |
| COS | 0.0005 | 0.0005 | 0.0005 | 0.0004 | 0.0004 | 0.0004 |
| $N_2$ | 0.0182 | 0.0182 | 0.0184 | 0.0154 | 0.0154 | 0.0155 |
| Exit Mass Flow, klb/hr | 543.63 | 542.09 | 538.96 | 502.30 | 502.18 | 501.02 |
| HHV of Syngas, Btu/lb | 4178.8 | 4139.4 | 4058.5 | 5198.7 | 5195.8 | 5166.1 |
| HHV of Syngas, Btu/SCF | 225.2 | 223.7 | 218.1 | 257.3 | 257.2 | 256.3 |
| Cold-Gas Efficiency, % | 76.0 | 75.1 | 73.2 | 87.4 | 87.3 | 86.6 |

Effect of Slurry Pre-Heat

There should be an advantage to pre-heating the slurry fed to the gasifier. Use of a "cold" slurry feed requires that heat generated within the gasifier from the fuel conversion process be used to vaporize the liquid water used to transport the coal. As noted in [Holt, 2001a], pre-heating the slurry before injection into the gasifier should increase the thermal efficiency of the gasifier and thereby provide a means to increase the carbon conversion within the gasifier, or allow reducing the size of the gasifier if the same carbon conversion is desired. For systems with cold or warm gas clean-up, the slurry pre-heat can potentially be performed by passing the hot syngas exiting the gasifier through a heat exchanger that pre-heats the incoming cold slurry prior to injection to the gasifier. For the gasifier at the Polk Power Station there is no slurry pre-heat and the slurry enters the gasifier at ambient conditions (about 60 °F = 288 K). The gasifier at Wabash River uses a pre-heated slurry (about 350 °F = 450 K).

Listed in Table 11 is a summary of the predicted one stage performance using two different slurry-feed temperatures. The first case is for our baseline conditions in which a slurry pre-heat is used (slurry temperature = 422K). The second case, T = 278K, represents using ambient conditions, or no pre-heat. The model results indicate the desired trend on syngas production. Using slurry pre-heat results in increased carbon conversion, heating value and cold gas efficiency. Further studies are needed to determine if the magnitude of the improvement is reasonable.

Also listed in Table 11 is a summary of the predicted performance for the two stage gasifier performance for the same change in slurry feed temperatures. The predicted results are in effect the same, implying that for these conditions and geometry there would be no noticeable change in performance. When viewed with the results from the previous parametric test, it could be that we have selected a height for the gasifier that is sufficiently tall, or has a sufficiently long residence time, that the impact of operational changes is washed out by the exit of the gasifier.

Table 11. Effect of Slurry Pre-Heat

| | One Stage | | Two Stage | |
|---|---|---|---|---|
| Pre-Heat | Yes | No | Yes | NO |
| Slurry Temperature, K | 422 | 298 | 422.0 | 298.0 |
| Exit Temperature, K | 1922.7 | 1860.7 | 1594.9 | 1595.5 |
| Carbon Conversion, % | 97.15 | 96.35 | 99.32 | 99.49 |
| Exit LOI, % | 18.86 | 22.99 | 1.48 | 1.34 |
| PFR Residence Time, s | 0.653 | 0.677 | 1.520 | 1.521 |
| Mole Fraction: CO | 0.4217 | 0.4159 | 0.4541 | 0.4544 |
| $H_2$ | 0.2413 | 0.2411 | 0.3259 | 0.3260 |
| $H_2O$ | 0.2192 | 0.2204 | 0.1324 | 0.1322 |
| $CO_2$ | 0.0910 | 0.0957 | 0.0630 | 0.0628 |
| $H_2S$ | 0.0079 | 0.0079 | 0.0081 | 0.0081 |
| COS | 0.0005 | 0.0005 | 0.0004 | 0.0004 |
| $N_2$ | 0.0182 | 0.0183 | 0.0154 | 0.0154 |
| Exit Mass Flow, klb/hr | 542.09 | 540.44 | 502.18 | 502.34 |
| HHV of Syngas, Btu/lb | 4139.4 | 4092.9 | 5195.8 | 5199.7 |
| HHV of Syngas, Btu/SCF | 223.7 | 222.0 | 257.2 | 257.2 |
| Cold-Gas Efficiency, % | 75.1 | 74.0 | 87.3 | 87.4 |

Effect of Wet .vs. Dry Feed

The Texaco and E-Gas gasifiers used in the large scale IGCC plants in the USA (i.e., Polk Power, Wabash River and Eastman Chemical), all employ a water based slurry to transport the fuel into the gasifier chamber. In contrast, the gasifiers developed by Shell and by groups in Japan employ a dry feed system. Potential advantages to a dry feed system include greater cold gas efficiency and reduced oxygen requirements [Holt, 2001a]. The dry feed could be obtained by using nitrogen or possibly carbon-dioxide as a carrier gas. For IGCC plants using an oxygen blown gasifier the nitrogen stream can be obtained from the exhaust of the Air Separation Unit. Using nitrogen for the coal transport medium is not unique to coal gasification. Blast furnaces used in the steel industry employ nitrogen for coal transport through the coal injection lance located in the furnace tuyere.

Listed in Table 12 is a summary of the predicted performance for the one stage gasifier using wet and dry feed. In these tests, the wet feed case corresponds to the baseline simulation (coal-water slurry containing 74% solids) and the dry feed case employs nitrogen to transport the coal (0.1lb N2 per lb of coal). In both cases the fuel stream is assumed to be at the same temperature (T = 422K) and the coal is used "as received". For these simulations, the dry feed simulation shows only a small increase in carbon conversion. However, the syngas generated with the dry feed has a much higher mole fraction of CO. Likewise, the heating value of the syngas generated with dry feed is significantly greater than the heating value of the syngas generated by the wet feed. Although the syngas heating value increased for the dry feed, the lower syngas mass flow rate results in a slight reduction in the cold gas efficiency. In light of the substantial change in syngas composition between the different feeds, a potential question to address in future work would be the impact on downstream processes (e.g., gas clean up, gas turbines, fuel cells) due to using a dry feed.

Listed in Table 12 is a summary of the predicted performance for the two-stage gasifier using wet and dry feed. For the two simulations, again, the carbon conversion is quite close. The dry feed indicates a slight reduction in carbon conversion. However, as with the one stage gasifier, due to injecting less moisture to the system the syngas produced with the dry feed has a much higher mole fraction of CO and heating value as compared to the wet feed simulation. In addition, due to the reduced mass flow of syngas, the dry feed results in a lower cold gas efficiency.

Table 12. Effect of Wet vs Dry Feed

| | One Stage | | Two Stage | |
|---|---|---|---|---|
| Feed Condition | Wet | Dry (N2) | Wet | Dry (N2) |
| Exit Temperature, K | 1922.7 | 2361.2 | 1594.9 | 1831.1 |
| Carbon Conversion, % | 97.15 | 98.41 | 99.32 | 98.93 |
| Exit LOI, % | 18.86 | 11.54 | 1.48 | 0.97 |
| PFR Residence Time, s | 0.653 | 0.626 | 3.22 | 3.9 |
| Mole Fraction: CO | 0.4217 | 0.5670 | 1.52 | 1.591 |
| $H_2$ | 0.2413 | 0.2268 | 0.4541 | 0.5936 |
| $H_2O$ | 0.2192 | 0.0908 | 0.3259 | 0.3042 |
| $CO_2$ | 0.0910 | 0.0403 | 0.1324 | 0.0141 |
| $H_2S$ | 0.0079 | 0.0088 | 0.0081 | 0.0094 |
| COS | 0.0005 | 0.0009 | 0.0004 | 0.0007 |
| $N_2$ | 0.0182 | 0.0630 | 0.0154 | 0.0599 |
| Exit Mass Flow, klb/hr | 542.09 | 481.57 | 502.18 | 437.92 |
| HHV of Syngas, Btu/lb | 4139.4 | 4626.1 | 5195.8 | 5890 |
| HHV of Syngas, Btu/SCF | 223.7 | 259.9 | 257.2 | 305.1 |
| Cold-Gas Efficiency, % | 75.1 | 74.6 | 87.3 | 86.3 |

Effect of System Pressure

From a modeling perspective, altering the system pressure for a fixed geometrical configuration is a useful parametric study to investigate model behavior. However, it is of limited value for practical operation. In the plant design process, the system pressure for the gasifier is determined by the amalgamation of considerations for the many equipment and processes to be used in the IGCC plant. Once the operating pressure for the gasifier is determined, the gasifier is sized to provide the desired fuel conversion for the anticipated residence time and conditions within the gasifier. Thus, in real world operation, one would not (and could not safely) significantly alter the steady state pressure from the original design condition. However, on the computer such tests can be performed.

Listed in Table 13 is a summary of the predicted performance for the one stage gasifier for varying the system pressure within the gasifier. The selected pressures are 18, 30 and 70 atm. and correspond to (a) the baseline conditions for our Vision 21 reference condition, (b) approximately the system pressure used by current generation coal gasifiers used for power production (and for many DOE IGCC studies) and (c) approximately the pressure reported for coal gasifiers used at "coal-to-chemicals" plants. From the table it appears that the model predicts the expected trends. As the system pressure increases the average gas residence time increases due to the reduced average gas velocity. The slower gas velocities result in increased particle residence time which in turn results in increased carbon conversion. At 70 atm., the model predicts in effect complete conversion of the fuel. It is interesting to note that in this study the pressure was increased by almost a factor of four, but the syngas higher heating value and cold gas efficiency only increased by a few percentage points. Listed in Table 13 is a summary of the predicted performance for the two-stage gasifier for the same set of system pressures. From the table it appears that the model predicts the expected trends. As the system pressure increases the average gas residence time increases due to the reduced average gas velocity. The slower gas velocities result in increased particle residence time which in turn results in increased carbon conversion. At 70 atm., the model predicts in effect complete conversion of the fuel.

Table 13. Effect of Pressure

| | One Stage | | | Two Stage | | |
|---|---|---|---|---|---|---|
| Pressure, atm | 18 | 30 | 70 | 18 | 30 | 70 |
| Exit Temperature, K | 1922.7 | 1905.5 | 1934.6 | 1594.9 | 1590.7 | 1619.7 |
| Carbon Conversion, % | 97.15 | 98.95 | 99.99 | 99.32 | 99.65 | 99.85 |
| Exit LOI, % | 18.86 | 7.90 | 0.04 | 1.48 | 1.14 | 0.32 |
| PFR Residence Time, s | 0.653 | 1.093 | 2.512 | 1.520 | 2.540 | 5.881 |
| Particle Residence Time, s | 0.026 | 0.042 | 0.101 | 0.996 | 1.405 | 2.910 |
| Mole Fraction: CO | 0.4217 | 0.4276 | 0.4324 | 0.4541 | 0.4548 | 0.4563 |
| $H_2$ | 0.2413 | 0.2481 | 0.2505 | 0.3259 | 0.3261 | 0.3231 |
| $H_2O$ | 0.2192 | 0.2100 | 0.2062 | 0.1324 | 0.1312 | 0.1327 |
| $CO_2$ | 0.0910 | 0.0876 | 0.0842 | 0.0630 | 0.0628 | 0.0616 |
| $H_2S$ | 0.0079 | 0.0079 | 0.0080 | 0.0081 | 0.0082 | 0.0082 |
| COS | 0.0005 | 0.0005 | 0.0005 | 0.0004 | 0.0004 | 0.0004 |
| $N_2$ | 0.0182 | 0.0181 | 0.0180 | 0.0154 | 0.0154 | 0.0154 |
| Exit Mass Flow, klb/hr | 542.09 | 545.77 | 547.90 | 502.18 | 502.90 | 503.29 |
| HHV of Syngas, Btu/lb | 4139.4 | 4234.0 | 4290.3 | 5195.8 | 5210.7 | 5217.8 |
| HHV of Syngas, Btu/SCF | 223.7 | 227.6 | 230.0 | 257.2 | 257.6 | 257.8 |
| Cold-Gas Efficiency, % | 75.1 | 77.3 | 78.7 | 87.3 | 87.7 | 87.9 |

Effect of Reaction Kinetics for Same Fuel

As discussed in the previous section on reaction kinetics (see above), the choice in reaction kinetics can have a significant impact on predicted values for a computational model. This can be especially important if computational models are used to help guide the sizing and design of gasification equipment. Unfortunately, there remains much work to be performed to establish reliable, general-purpose rules and correlations that analysts can use to estimate kinetic parameters for different coals for gasification applications.

To demonstrate the impact of using different kinetics, in this section we compare solutions predicted using two kinetic sets from the literature. The tests are performed using kinetic parameters developed by [Lupa and Kliesh, 1979] and [Roberts and Harris, 2000]. The kinetic parameters by [Lupa and Kliesh, 1979] were developed for Illinois #6 coal across a range of temperatures and pressures representative of gasification conditions. These are the same kinetic parameters as used in the baseline simulation. The kinetic parameters taken from [Roberts and Harris, 2000] are for an Australian coal (coal Y) with properties comparable to Illinois #6, for tests performed at 10 atm. Comparing the two sets of kinetics, for high temperatures and pressures the two kinetic sets are comparable for combustion ($C+O_2$) reactions but for gasification reactions ($C+CO_2$, $C+H_2O$) the baseline kinetic set is at least an order of magnitude faster than that of [Roberts and Harris, 2000].

Listed in Table 14 is the predicted performance for the one stage gasifier for using the two sets of kinetic parameters. In this test, the coal kinetics were the only model input parameters changed. Comparing the simulation results, it can be seen that the two parameter sets predict very different behavior. Using the parameters by Roberts and Harris results in a significantly lower carbon conversion. As a result, the carbon-in-ash (LOI) is much higher and the syngas mass flow rate, heating value and cold gas efficiency are much lower.

Listed in Table 14 is the predicted performance for the two-stage gasifier using the two sets of kinetic parameters. The impact of the different kinetics is not as severe for this gasifier as it was

Table 14. Effect of kinetics

| | One Stage | | Two Stage | |
|---|---|---|---|---|
| Reaction Kinetics Set | Lupa and Kliesh | CCSD | Lupa and Kliesh | CCSD |
| Exit Temperature, K | 1922.7 | 2135.5 | 1594.9 | 1759.8 |
| Carbon Conversion, % | 97.15 | 84.93 | 99.32 | 94.01 |
| Exit LOI, % | 18.86 | 55.13 | 1.48 | 30.80 |
| PFR Residence Time, s | 0.653 | 0.647 | 1.520 | 1.441 |
| Mole Fraction: CO | 0.4217 | 0.3772 | 0.4541 | 0.4434 |
| $H_2$ | 0.2413 | 0.1900 | 0.3259 | 0.3036 |
| $H_2O$ | 0.2192 | 0.2886 | 0.1324 | 0.1625 |
| $CO_2$ | 0.0910 | 0.1159 | 0.0630 | 0.0662 |
| $H_2S$ | 0.0079 | 0.0066 | 0.0081 | 0.0080 |
| COS | 0.0005 | 0.0005 | 0.0004 | 0.0004 |
| $N_2$ | 0.0182 | 0.0195 | 0.0154 | 0.0158 |
| Exit Mass Flow, klb/hr | 542.09 | 517.16 | 502.18 | 491.54 |
| HHV of Syngas, Btu/lb | 4139.4 | 3461.1 | 5195.8 | 4916.8 |
| HHV of Syngas, Btu/SCF | 223.7 | 195.3 | 257.2 | 246.8 |
| Cold-Gas Efficiency, % | 75.1 | 59.9 | 87.3 | 80.9 |

for the one stage configuration. Using the parameters by Roberts and Harris results in a noticeably lower carbon conversion. As observed in other simulations, the lower carbon conversion results in a higher exit gas temperature. Compared to the baseline, the LOI is much higher and the syngas mass flow rate, temperature, heating value and cold gas efficiency are much lower.

The results of this parametric test emphasize the importance of using the best available reaction kinetics.

Effect of Fuel Switching

The economics of operating an IGCC plant require that the operator have the flexibility to switch fuels and maintain good gasifier performance. As an example, the Polk Power Station has operated with over twenty different solid fuels since startup [Hornick, 2002]. However fuel switching is not a trivial process. The new fuel must maintain the required syngas production and good slagging properties must be maintained to protect the refractory from excessive wear.

Gasifier simulations have been performed using three different solid fuels: Illinois #6, Power River Basin (PRB) and Petcoke. All three fuels have been used in commercial scale gasifiers. The Petcoke and PRB are popular in some regions of the USA due to their low price. All three simulations were performed using the same model inputs, excepting for fuel composition (see Table 3) and kinetic parameters. The kinetic parameters for Illinois #6 are the same as used in the baseline simulation [Lupa and Kliesh, 1979]. The kinetics for Petcoke were estimated by using the values from Lupa and Kliesch and reducing these by a factor of five. The kinetic parameters for PRB were estimated in a similar manner, but by multiplying by a factor of five.

Table 15. Effect of Fuel Type - One Stage Only

| Fuel Type | Illinois#6 | Petcoke | PRB |
|---|---|---|---|
| Exit Temperature, K | 1922.7 | 2327.3 | 1700.7 |
| Carbon Conversion, % | 97.15 | 99.38 | 91.40 |
| Exit LOI, % | 18.86 | 52.28 | 54.15 |
| PFR Residence Time, s | 0.653 | 0.562 | 0.754 |
| Mole Fraction: CO | 0.4217 | 0.4991 | 0.3521 |
| $H_2$ | 0.2413 | 0.2180 | 0.2246 |
| $H_2O$ | 0.2192 | 0.1782 | 0.2738 |
| $CO_2$ | 0.0910 | 0.0734 | 0.1297 |
| $H_2S$ | 0.0079 | 0.0096 | 0.0016 |
| COS | 0.0005 | 0.0008 | 0.0001 |
| $N_2$ | 0.0182 | 0.0177 | 0.0181 |
| Exit Mass Flow, klb/hr | 542.09 | 546.63 | 530.39 |
| HHV of Syngas, Btu/lb | 4139.4 | 4294.5 | 3535.0 |
| HHV of Syngas, Btu/SCF | 223.7 | 240.4 | 195.1 |
| Cold-Gas Efficiency, % | 75.1 | 75.0 | 71.0 |

Listed in Table 15 is the predicted gasifier performance for the three fuels. Comparing the results it can be seen that the different fuels produce syngas with quite different compositions, quality, heating value and cold gas efficiency. Relative to the performance of Illinois #6 (baseline), the Petcoke resulted in higher carbon conversion. The LOI of the flyash appears high due to the very small amount of ash in the Petcoke making any carbon in the flyash appear as a large LOI value. Compared to the baseline, the Petcoke resulted in a significantly higher exit temperature due to the high amount of carbon and relatively few dilatants in Petcoke. The predicted CO concentration in the syngas generated by Petcoke is much higher than that for Illinois #6. Likewise, the predicted heating value (Btu/SCF) for Petcoke is noticeably greater than for Illinois #6. However, the cold gas efficiency

is lower than for Illinois #6 due to the much higher heating value of Petcoke in as received form. Comparing the predicted values for the Illinois # 6 and PRB, the syngas generated with PRB has somewhat lower carbon conversion, and a noticeably lower CO concentration, heating value and cold gas efficiency.

The results of this test should not be interpreted to indicate that one fuel might be better than another for gasifier applications. Such a comparison will require a more in-depth analysis than performed here. In particular, more thought needs to be invested on how to modify the operating conditions (e.g., oxygen and steam flows) to match the syngas produced for the baseline operation. With such a comparison, then the criteria to judge the benefit (if any) of using different fuels could be limited to the differential cost to operate at the required conditions and the impact on slag management and refractory wear.

Effect of Gasifier Length

An advantage to using computational models is that it provides a means to "easily" explore the impact on performance of altering the size, shape or volume of the gasifier.

Listed in Table 16 is the predicted gasifier performance for the baseline configuration and two alternative gasifier sizes. For simplicity, in this study we only change the gasifier length. The three simulations correspond to the gasifier having a L/D ratio = 1, 2 (baseline) and 3. Comparing the predicted values, the expected trends are observed. As the gasifier increases in length, the predicted carbon conversion, mean particle residence time, syngas heating value and cold gas efficiency increase correspondingly. In addition, note that for L/D = 1, the predicted carbon conversion is in excess of 90% suggesting that most of the fuel conversion happens very rapidly within the gasifier.

Table 16. One Stage Gasifier – Effect of length

| Gasifier Length (L/D ratio) | 1 | 2 (baseline) | 3 |
|---|---|---|---|
| Exit Temperature, K | 2021.9 | 1922.7 | 1870.2 |
| Carbon Conversion, % | 92.72 | 97.15 | 99.27 |
| Exit LOI, % | 37.25 | 18.86 | 5.41 |
| PFR Residence Time, s | 0.332 | 0.653 | 0.969 |
| Mole Fraction: CO | 0.4081 | 0.4217 | 0.4274 |
| $H_2$ | 0.2232 | 0.2413 | 0.2506 |
| $H_2O$ | 0.2429 | 0.2192 | 0.2071 |
| $CO_2$ | 0.0984 | 0.0910 | 0.0882 |
| $H_2S$ | 0.0074 | 0.0079 | 0.0079 |
| COS | 0.0005 | 0.0005 | 0.0005 |
| $N_2$ | 0.0187 | 0.0182 | 0.0180 |
| Exit Mass Flow, klb/hr | 532.72 | 542.09 | 546.42 |
| HHV of Syngas, Btu/lb | 3906.5 | 4139.4 | 4249.7 |
| HHV of Syngas, Btu/SCF | 212.7 | 223.7 | 228.0 |
| Cold-Gas Efficiency, % | 69.7 | 75.1 | 77.7 |

## Preliminary Gasifier Calculations - *AIOLOS*

The work during the last performance period has been focused on the definition of a single stage industrial gasifier configuration, and on the generation of steady state results for this configuration. Simulations have been performed for the one-stage, downfired gasifier (see Figure 16) for the baseline operating conditions used for the ***GLACIER*** simulations with 70% load. Illustrated in Figures 24 and 25 are the predicted $O_2$, $H_2$, CO and $CO_2$ concentrations for a representative plane passing through the centerline of the gasifier. From the figures a symmetric flow field can be observed. Table 17 shows the syngas composition and the exit conditions.

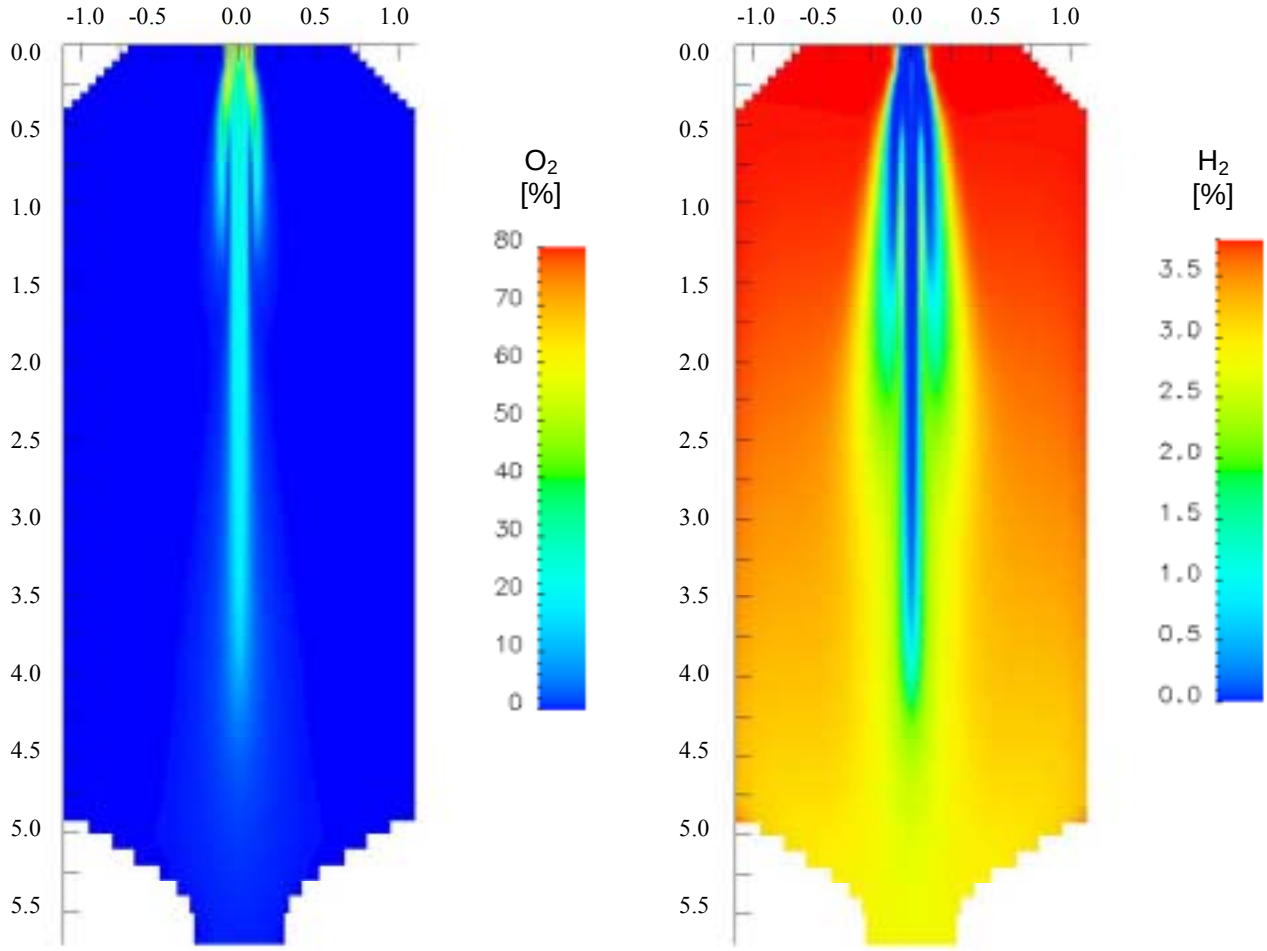


Figure 24. Computational results of the $O_2$- (left) and $H_2$-distribution (right).

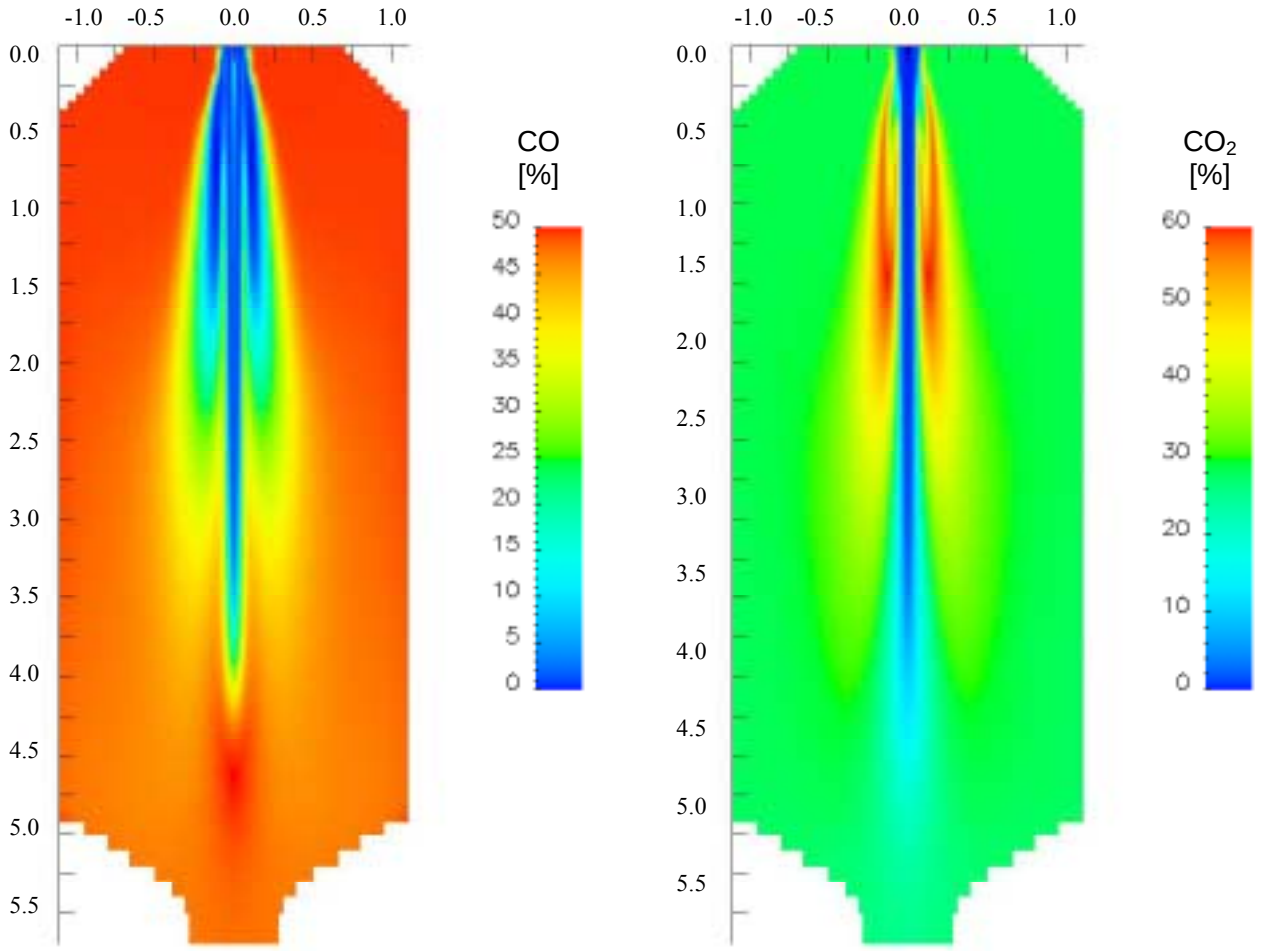


Figure 25. Computational results of the CO- (left) and $CO_2$-distribution (right).

Table 17. One Stage Gasifier – Baseline Exit Conditions

| | |
|---|---|
| Exit Temperature, K | 1509.0 |
| Exit LOI, % | 2.55 |
| Mole Fraction: CO | 0.3788 |
| $H_2$ | 0.3046 |
| $H_2O$ | 0.0882 |
| $CO_2$ | 0.1369 |
| $CH_4$ | 0.0443 |
| HHV of Syngas, Btu/lb | 4896.0 |

# Conclusions

During the last quarter good progress has been made on the development of our IGCC workbench. A series of parametric CFD simulations for one stage and two stage "generic" gasifiers using firing conditions based on the Vision 21 reference configuration have been performed. A flowing slag model has been implemented into the CFD based gasifier model and is in the process of being tested. A review of the available reaction kinetics for coal under high pressure and high temperature conditions for gasification conditions has been performed. Many of the reactor models required to simulate the heat transfer and gas clean up equipment downstream of the gasifier have been developed and implemented into the workbench. A tool to allow "stretching" the provided geometry of the one and two stage gasifier has been implemented into the workbench. Software enhancements to allow implementing to the workbench a reactor model using the CAPE_Open software interface protocol has commenced.

Plans for the next quarter include: further development of the CFD gasifier models, with special focus on reaction kinetics, the slagging wall model and additional parametric cases; developing or acquiring models needed to simulate equipment and processes downstream of the gasifier for the energyplex reference configuration; and implementing modifications to the workbench software infrastructure to support further development of the IGCC workbench, such as the use of the CCA and CAPE_Open software interface protocols.

# References

Anthony D.B. and Howard J.B., Coal devolatilization and hydrogasification, *AIChE J*., **22,** 625-656, 1976.

Arendt P. and van Heek K.H., Comparative investigations of coal pyrolysis under inert gas and $H_2$ at low and high heating rates and pressures up to 10 MPa, *Fuel*, **60,** 779-787, 1981.

Banin et al., *Combustion and Flame*, **108**, 1-8, 1997.

Beath A.C., Mathematical modeling of entrained flow gasification, PhD thesis, University of Newcastle, Australia, 1996.

Benfell, K. E., Liu, G.-S., Roberts, D. G., Harris, D. J., Lucas, J. A., Bailey, J. D., and Wall, T. F., *Proceedings of the Combustion Institute,* **28**, 2233-2241, 2000.

Benyon, P., Inumaru, J., Otaka, M., Hara, S., Watanabe, H. and Kent J. Engineering Modelling of High Pressure and Temperature Entrained-Flow Gasifiers. *Japan-Australia Joint Technical Meeting on Coal*, December 5-6, 2000, Fukuoka, Japan.

Benyon P.J., Computational modeling of entrained flow slagging gasifiers, PhD thesis, University of Sydney, Australia, 2002.

Bockelie, M.J., Adams, B.R., Cremer, M.A., Davis, K.A., Eddings, E.G., Valentine, J.R., Smith, P.J., and Heap, M.P., Computational simulations of industrial furnaces, Proceedings of the

International Symposium on Computational Technologies For Fluid/Chemical Systems with Industrial Applications, Joint ASME/JSME Conference, San Diego, CA, 1998.

Bockelie, M.J., Swensen, D.A., Denison, M.K., Sarofim, A.F., "A Computational Workbench Environment For Virtual Power Plant Simulation," presented at the Vision 21 Program Review Conference, Morgantown, WV, Nov. 6-7, 2001.

Bockelie, M.J., Swensen, D.A., Denison, M.K., Chen, Z., Senior, C.L., Sarofim, A.F., A Computational Workbench Environment for Virtual Power Plant Simulation, *Proceedings of the 27th International Technical Conference on Coal Utilization and Fuel Systems*, Clearwater, FL, USA, March 4-7, 2002.

Bockelie, M.J., Swensen, D.A., Denison, M.K., Chen, Z., Senior, C.L., Sarofim, A.F., "A Computational Workbench Environment for Virtual Simulation of a Vision 21 Energyplex", *Proceedings of the ASME International Joint Power Generation Conference 2002,* Phoenix, AZ, USA, June 24-27, 2002.

CCSD. URL = http://www.newcastle.edu.au/research/centres/blackcoal.html.

Chen, C. Miyoshi, T., Kamiya, H., Horio, M., and Kojima, T., On the Scaling-up of a Two-Stage Air Blown Entrained Flow Coal Gasifier, *The Canadian Journal of Chemical Engineering*, **77**, 745-750, 1999.

Chen, C., Horio, M., and Kojima, T., Numerical Simulation of Entrained Flow Coal Gasifiers, *Chemical Engineering Science*, **55,** 3861-3883, 2000.

De Nevers, N., *Air Pollution Control Engineering*, 2d ed., McGraw-Hill, New York, Chapter 9, 2000.

DOE-NETL, Texaco Gasifier IGCC Base Cases, PED-IGCC-98-001, July 1998, Latest Revision, June 2000a.

DOE-NETL, DESTEC Gasifier IGCC Base Cases, PED-IGCC-98-003, September 1998, Latest Revision, June 2000b.

Fletcher T.H., Kerstein A.R., Pugmire R.J. and Grant D.M., *Energy & Fuels*, **4**, 54, 1990.

Gibbins J.R. and Kandiyoti R., The effect of variations in time-temperature history on product distribution from coal pyrolysis, *Fuel*, **68,** 895-903, 1989.

Griffin T.P., Howard J.B. and Peters W.A., Pressure and temperature effects in bituminous coal pyrolysis: experimental observations and a transient lumped-parameter model, *Fuel*, **73**, 591-601, 1994.

Harris D.J., Kelly M.D., Roberts D.G., Mill C.J., Stubington J.F. and Wall T.F., Determining coal reactivity parameters at elevated pressures using bench-scale techniques, 2002.

Harris, D. J., and Smith, I. W., *Proceedings of the Combustion Institute*, **23**, 1185-1190, 1990.

Holt, N., Integrated Gasification Combined Cycle Power Plants, unpublished manuscript, March, 2001a.

Holt, N., Coal Gasification Research, Development and Demonstration – Needs and Opportunities, presented at the *Gasification Technologies 2001 Conference*, San Francisco, CA, Oct. 8-10, 2001b.

Hornick, M., Polk Power Station IGCC, *Proceedings of the 27th International Technical Conference on Coal Utilization and Fuel Systems*, Clearwater, FL, USA, March 4-7, 2002.

Hoy, H.R., Roberts, A.G. and Wilkins, D.M., Behavior of mineral matter in slagging gasification processes. *J. Inst. Gas Engrs,* **5**, 444, 1965.

Hurt, R., Sun, J-K, Lunden, M., *Combustion and Flame,* **113**, 181, 1998.

IEA, *Modeling and Simulation for Coal Gasification*, IEA Coal Research 2000, ISBN 92-9029-354-3, December, 2000.

Joutsenoja et al., *Energy and Fuels*, **13**, 130-145, 1999.

Kobayashi, H., Howard, J.B. and Sarofim, A.F., Coal devolatilization at high temperatures, *6th Symposium (Int) on Combustion*, The Combustion Institute, 411-425, 1976.

Kunii, D., and Levenspiel, O., *Fluidization Engineering*, John Wiley and Sons Inc., 1969, pp 698-699.

Liu, G., Benyon, P., Benfell, K.E., Bryant, G.W., Tate, A.G., Boyd, R. K., Harris, D.J., and Wall, T.F., *Fuel*, **79**, 617-626, 2000.

Lupa and Kliesch, Simulation of a Texcao Gasifier, Vol.1 A Steady State Model, EPRI Report AF-1179, Vol. 1 Research Project 1037-1. Final Report, 1979.

Monson et al., *Combustion and Flame*, **100**, 669-683, 1995.

Niksa S. and Kerstein A.R., FLASHCHAIN theory for rapid coal devolatilization kinetics 1. Formulation, *Energy & Fuels*, **5**, 673-683, 1991.

NRC, *Coal - Energy for the Future*, National Academy Press, Washington, DC, 1995.

Okumura Y., Sugiyama Y. and Okazaki K., Evolution behavior of coal-nitrogen in high pressure pyrolysis processes, *Fuel Chemistry Division Preprints*, **46**, 141-143, 2001.

Otaka et al., the 26th International Conference on Coal Utilization and Fuel Systems, Clearwater, Fl., 2001.

Patterson, J.H. Hurst, H.J. Quintanar, A. Boyd, B.K. and Tran, H. Evaluation of the slag flow characterization of Australian coals in slagging gasifiers. *Research Report 19, Volume 1. Cooperative Research Centre for Black Coal Utilisation*, University of Newcastle, Australia, May, 2001.

REI_Models. URL http://www.reaction-eng.com.

Roberts, D.G. and Harris, D.J., Char gasification with O2, CO2, and H2O: Effects of pressure on intrinsic reaction kinetics, *Energy & Fuels*, **14**, 483-489, 2000.

Roberts, D.G., Harris, D. J., and Wall, T. F., High-Pressure Intrinsic Char Gasification Kinetics: an Application of a modified nth-order rate equation, the 18th Pittsburgh Coal Conference, Newcastle, Australia, 3-7 Dec, 2001.

Rodgers, M.W., Slag layers in coal-fired MHD generators. *PhD thesis*, Stanford University, Palo Alto, CA, 1979.

Seggiani, M., Modelling and simulation of the time varying slag flow in a Prenflo entrained-flow gasifier. *Fuel*, **77**, 1611, 1998.

Senior, C.L. and Sangiovanni, J.J., Numerical model of slag flow in a novel coal-fired furnace, *International Journal of Heat and Mass Transfer*, 2001.

Senneca, O., Salatino, P., Masi, S., *Fuel*, **77**, 1483, 1998.

Shelton, W., and Lyons, J., Texaco Gasifier IGCC Base Cases, US DOE / NETL report number PED-IGCC-98-001, July 1998, Latest Revision June 2000.

Smith I.W., The combustion rates of coal chars: a review, *Proceedings of the Combustion Institute*, 1045-1065, 1982.

Smoot, L.D. and Smith, P.J., *Coal Combustion and Gasification*, Plenum Press, NY, NY 1985.

Solomon P.R., Hamblen D.G., Carangelo R.M., Serio M.A. and Deshpande G.V., General model of coal devolatilization, *Energy & Fuels*, **2**, 405, 1988.

Solomon P.R., Serio M.A. and Suuberg E.M., Coal pyrolysis: experiments, kinetic rates and mechanisms, *Prog. Energy Combustion Sci*., **18**, 133-220, 1992.

Steigel, G.J., Clayton, S.J., and Wimer, J.G., DOE's Gasification Industry Interviews: Survey of Market Trends, Issues, and R&D Needs, presented at the *Gasification Technologies 2001 Conference*, San Francisco, CA, Oct. 8-10, 2001.

Suuberg E.M., Peters W.A. and Howard J.B., Product compositions and formation kinetics in rapid pyrolysis of pulverised coal - implications for combustion, *Proceedings of the Combustion Institute*, **17,** 117-128, 1978.

Tilton, J. N. , "Fluid and Particle Dynamics," in *Perry's Chemical Engineers' Handbook* 7th ed., R. H. Perry, D. W. Green, eds., McGraw-Hill, New York, 1997, Sec. 6, p. 11.

Urbain, G., Cambier, F., Deletter, M., and Anseau, M.R., Viscosity of Silicate Melts. *Trans. J. Br. Ceram. Soc.*, **80**, 139, 1981.

Wall T.F., Liu G.-S., Wu H.-W., Roberts D.G., Benfell K.E., Lucas J.A. and Harris D.J., The effect of pressure on coal reactions during pulverized coal combustion and gasification, to be published, 2002.

Watt, J.D., The flow properties of slags formed from the ashes of British coals: Part 2. The crystallizing behavior of the slags. *J. Inst. Fuel*, **42**, 131, 1969.

Wen, C.Y., and Galli, A.F., "Dilute Phase Systems," in *Fluidization*, Davidson, J.F., and Harrison, D., eds., Academic Press Inc., London, 1971, pp 698-699.

Wen C.Y. and Chaung T.Z., Entrained coal gasification modeling, *Ind. Eng. Chem. Process Des. Dev.,* **18**, 684-695, 1979.

Wu, H., Bryant, G. W., and Wall, T. F., *Energy and Fuels*, **14**, 745-750, 2000.